First geoarchaeological study of a Palaeolithic site on the northern edge of the Iranian Central Desert: Mirak (Semnan, Iran)

Mohammad Akhavan Kharazian, Guillaume Jamet, Simon Puaud, Hamed Vahdati Nasab, Milad Hashemi, Guillaume Guerin, Maryam Heydari, Pierre Antoine, Jean-Jacques Bahain, Gilles Berillon

First geoarcheological study of a Palaeolithic site on the northern edge of the Iranian Central Desert: Mirak (Semnan, Iran)

Mohammad Akhavan Kharazian[a,*], Guillaume Jamet[b,c], Simon Puaud[d], Hamed Vahdati Nasab[e], Milad Hashemi[e], Guillaume Guerin[f], Maryam Heydari[f], Pierre Antoine[c], Jean-Jacques Bahain[d], Gilles Berillon[d],

a: Ecole doctorale Géographie (UFR 08), Université Paris 1 Panthéon Sorbonne, Paris, France
b: GéoArchÉon Viéville-sous-les-Côtes, France
c : UMR 8591 Laboratoire de Géographie Physique Pierre Birot CNRS-Université Paris 1, Meudon, France
d: UMR7194 HNHP MNHN-CNRS-UPVD / Département Homme et Environnement, Musée de l'Homme, Paris, France
e: Department of Archaeology, Tarbiat Modares University, Tehran, IRAN
f: UMR 5060 IRAMAT-CRP2A / Université Bordeaux Montaigne, Maison de l'Archéologie, Pessac, France

Abstract

Mirak is a Palaeolithic site in Iran comprising several localities ("mounds") scattered over a dry floodplain environment extending from the southern foothills of the Alborz Mountains to the northern edge of the Central Desert in the Semnan area. The area has been studied since 2015 by an Iranian-French archaeological mission. The archaeological excavations carried out at the Mirak N°8 mound uncovered a 7 m-thick pedo-sedimentary sequence, in which two sequences corresponding to contrasting depositional environments have been observed. Sequence I, comprising alternating horizons of poorly pedogenised clayey silt intercalated with sand layers, is interpreted as an alluvial pedo-sedimentary body deposited in a wetland (floodplain) environment during cold periods, periodically interrupted by shallow sheet flooding deposits. According to the stratigraphy, OSL dates and sedimentological analyses, there is a long sedimentary hiatus before the occurrence of sequence II which corresponds to calcareous aeolian deposits typical of a desert environment. The Mirak N°8 deposits were affected by several stages of incipient aridisol formation with desiccation cracks implying a gradually increasing prevalence of more arid conditions. According to the OSL data, the Mirak N°8 sequence was deposited from the Late Pleistocene to the Late Holocene (52ka to 0.4ka). In this sequence, upper Palaeolithic remains were recovered at distinct levels and it can be presumed that the most recent archaeological layer is made up of palimpsests resulting from repeated human occupations.

Results from various mineralogical and sedimentological analyses (XRD, FTIR, SEM, optical microscopy) show very minor differences in mineralogy throughout the record regardless of the type of depositional regime, suggesting a local, and most probably polygenic, sedimentary source. Both alluvial and aeolian accumulations were subjected after deposition to a variety of post-sedimentary pedogenesis processes indicated by pedogenic features characteristic of calcareous, gypsiferous aridisols (Bk, By), including ferruginous root coatings, evaporates and little-developed pedo-structures and horizons. Apparent differences in colour between the two sequences at Mirak N°8 can be attributed to deposition in environments with varying iron contents and oxygenizing conditions, presumably related to higher groundwater levels and Fe-reducing conditions, especially for the units deposited during the late Pleistocene as opposed to the generally warm and dry conditions of the Holocene.

Key words: Iran; Mirak; Palaeolithic; Geoarchaeology, Quaternary.

Introduction

To gain a clear and comprehensive understanding of the palaeoenvironment of archaeological sites, archaeological studies have to be combined with approaches from geoscience. However, in most older archaeological projects in Iran, this multidisciplinary geoarchaeological approach has usually not been taken into account or simply assumed to be unnecessary, and this is a matter to be heeded more seriously in future. Despite this, several stand-alone and often high-resolution pedo-stratigraphical, palynological and geochronological explorations focusing on palaeoclimatic reconstruction of the Quaternary era have been carried out in some regions of the Iranian plateau. They have produced a broad (due to the vast extent and geomorphological diversity of Iranian landscapes), but informative picture of the region's palaeoclimatic history. These palaeoclimatic studies in Iran have covered a variety of morpho-sedimentary contexts including lacustrine deposits (e.g. Van Zeist and Wright, 1963; Bottema, 1986; Kelts and Shahrabi, 1986; Griffiths et al., 2001; Stevens et al. 2006; Djamali et al., 2008; 2009; Ramezani et al., 2008; Leroy et al., 2013; Sharifi et al., 2015, Hamzeh et al., 2016), loess-palaeosol sequences (e.g. Lateef, 1988; Kehl et al., 2005; 2009b; Berillon et al., 2007; Frechen et al., 2009; Wang et al., 2016; Taheri et al., 2017; Lauer et al., 2017; Vlaminck et al., 2018) and playas and alluvial contexts (e.g. Krinsley, 1970; Weise, 1974; Regard et al., 2006; Bayat et al., 2018; Vaezi et al., 2019) (Fig. 1).

[Figure 1 about here; in black and white]

In Iranian territory, it is generally difficult to show evidence of Quaternary sequences that can be fully and accurately correlated with global palaeoclimatic records (Kehl, 2009a). However, periodic warm/cold changes during the Quaternary have often produced meaningful patterns in pedo-sedimentary sequences. For instance, there seems to be a wide consensus that, at least in central, western and northern Iran, warm and relatively moist conditions resulted in soil formation during interglacials/interstadials, whereas cold and arid conditions caused a predominance of aeolian dust deposition during glacials/stadials. In this context, palaeoclimatic interpretations of Late Pleistocene formations in Iran are mostly deduced from investigations carried out on the loess-palaeosol sequences (LPS) located along the Alborz Range in the north and the Kopeh Dagh Mountains in north-eastern Iran (e.g. Kehl et al., 2005, Frechen et al., 2009, Vlaminck et al., 2018).

During the Late Pleistocene, relatively colder and drier overall climatic conditions than today's dominated parts of southern Eurasia, including northern and north-eastern Iran, along with intermittent occurrences of moist and relatively warmer episodes during the last interglacial (MIS5e/Eemian) and the various interstadials of the last glacial (Vlaminck et al., 2018). Based on isotopic investigations of cave stalagmites, it has been proposed that an increase in solar insolation during the last interglacial triggered higher precipitation rates in central north-western Iran (Mehterian et al., 2017). Sedimentological and chronological studies of aeolian deposits on the Iranian loess plateau (e.g. Wang et al., 2016; Taheri et al., 2017; Lauer et al., 2017) substantiate the possibility of a trend towards aridification around the end of Late Pleistocene. Well-documented lacustrine records such as those from Lake Urmia in north-west Iran (Djamali et al., 2008), Lake Mirabad and Lake Zaribar in the Zagros (Zeist and Bottema, 1977; 1991;

Stevens et al., 2001; 2006; Lambert, 2010) and, on a supra-regional scale, Lake Van in Turkey (Litt et al., 2014) allow a more precise reconstruction of the palaeoclimatic conditions in Iran during the Late Pleistocene. The frequency of pollen species found in sediment cores from these lakes indicate a slightly warmer and moister climate during the Eemian, whereas the abundance of steppe species such as *Artemisia* represents a drier and relatively colder climate during the Late Pleniglacial and the Lower Holocene (MIS 1). Even though the sedimentological and pollen records provide a picture of analogous palaeoclimatic conditions for the Late Pleistocene in the mountainous regions of western Iran, the same conditions cannot be attributed with confidence to the lowlands of the central Iranian zone. Except for a very few investigations in scattered locations in the central Iranian zone (e.g. Thomas et al., 1997; Kehl et al., 2005; Bayat et al., 2019), Pleistocene and Holocene palaeoclimatic and palaeoenvironmental studies, especially on sub-desert and desert areas south of the Alborz and east of the Zagros Range, do not exist at present.

The end of the Pleniglacial and the onset of the Late Glacial (MIS 1) is mostly described as a stage of increasing dryness and relatively colder climatic conditions in Iran (e.g. Wasylikowa et al., 2006; Djamali et al., 2008; Kehl et al., 2009a) and the Near East (Van Zeist and Bottema, 1991; Pickarski et al., 2015). This transition was not limited to the mountainous regions only and is reflected as episodes of extensive erosion or/and dust deposition in the results from palaeoclimatic investigations in the more southerly territories of Iran as well (e.g. Bogemans, 2017; Vaezi et al., 2019).

Dispersion and migration routes of Late Pleistocene hunter-gatherer populations across the Iranian plateau are always discussed in studies of the area's prehistoric sites (see Vahdati Nasab et al, 2019 for a synthesis). Given the widespread distribution of Palaeolithic sites (Vahdati Nasab et al., 2013) thus far, several models of dispersal have been proposed by researchers (see Shoaee et al., 2021 for a review). These hypotheses are generally based on geography, location of Palaeolithic sites and the palaeoenvironment. However, few Palaeolithic studies have presented their archaeological arguments within a clear and precise environmental and geochronological framework. A clearer and more reliable understanding of the palaeoenvironment and the geological evolution of archaeological sites can provide new perspectives and lay more solid ground for hypotheses on dispersion and migration.

In order to address our inadequate and patchy knowledge of the palaeoenvironment of central Iran during the Late Pleistocene, a well-excavated and well-documented archaeological site in this region, such as Mirak, offers a remarkable opportunity. Mirak is an open-air prehistoric site located in the Delazian region, 8 kilometres south of the modern city of Semnan (220 km east of Tehran) in the northern portion of Iran’s Central Desert or *Dasht-e-Kavir*. It was discovered in 1989 (Rezvani, 1990) and its potential was revealed much later through a systematic prospecting campaign (Vahdati Nasab, 2009). The archaeological survey of the surface of eight natural mounds scattered across the study area (numbered Mirak N°1 to Mirak N°8) resulted in a collection of thousands of lithic artefacts (more than 7700 during the 2009 excavation), whose quantity and characteristics made Mirak a potentially major Middle Palaeolithic site in the central Iranian zone (Rezvani and Vahdati Nasab, 2010; Vahdati Nasab et al., 2013). So far,

archaeological excavations in the Mirak area have focused on the Mirak mound N°8 site, which has the highest lithic density on the surface. This site has the shape of a mound about 5m in height, which has been interpreted as a Holocene dune on top of Pleistocene deposits (Vahdati Nasab et al., 2019). Excavation of the Pleistocene deposits have uncovered at least three main archaeological layers which, culturally, appear to correspond to at least three main phases of human occupation dating back 26 to 55 ka (Vahdati Nasab et al., 2019; Heydari et al., 2020). The lithic assemblage of the upper layer (L1, 21-28 ka), although not well preserved, shows some Upper Palaeolithic affinities. The intermediate layer (L2, 26–33 ka) indicates singular characteristics in the Iranian Central Plateau with a mix of industries with both Upper and Middle Palaeolithic affinities. The lower layer (L3, 55-44 ka) has clear Middle Palaeolithic affinities, which appear to be very recent for the area. In general, the Mirak industries raise questions over the cultural diversity of the area lying between the Zagros and Central Asia.

The Franco-Iranian team working under the "FIPP" palaeoanthropological program has conducted multidisciplinary studies in the Mirak region since 2015. Geoarchaeological and geochronological investigations were carried out at the site in addition to archaeological studies. Several scientific papers on the palaeoanthropology of the archaeological finds and dating of the Mirak N°8 site have been published (e.g. Berillon et al., 2015; 2016; 2017; Heydari et al., 2020). This study presents the results of high-resolution pedo-stratigraphical studies and physico-chemical analyses of the Mirak N°8 sequence and proposes a new pedo-stratigraphic and archaeological reference for the last 50 ka in Central-NE Iran.

The study area: geographic, geomorphological and geological contexts

The open-air site of Mirak N°8 is located in a dry mudflat (53°25'53" E ; 35°28'10" N ; ca. 1035 m a.s.l) in the Semnan piedmont, about 16 km from the southern foothills of the Alborz Mountains and close to the northern edge of the Iranian Central Desert or *Dasht-e Kavir* (Fig. 1b). The piedmont corresponds to an elongated Quaternary drainage system in a context of intra-mountainous depression, within which streams ran southwards, forming alluvial fans, floodplains, and possibly parts of the saline playa-lakes downstream. The entire network of thalwegs, whether drained or not, originates in the Alborz massif and becomes concurrent where the Gey-No river, the largest permanent watercourse in the area and less than a kilometre to the east of Mirak N°8, becomes the main river system. The region extends over an area of 1.6 km².

From a geological point of view, the substratum is characterized by a series of Tertiary synclines and anticlines (Eocene to Miocene) covered by Plio-Pleistocene and Holocene formations (Haddadan et al. 1994). In this semi-sloping (about 0.9%) peri-desert plain, Mirak represents a system of small asymmetric mounds (4 to 11 m in height) (Fig. 2a), about a hundred metres apart at an altitude of 1100 m to 1000 m a.s.l. These mounds extend in a line for about 2.5 km, and their age and origin are not yet fully determined (Vahdati Nasab et al., 2013). To date, Mirak N°8 (Fig. 2b) is the only archaeological locality to have been geo-archaeologically studied.

Applying optically stimulated luminescence (OSL) dating to quartz grains resulted in the range of 55-44 ka to 28-21 ka during the Upper Pleistocene and 0.8-0.4 ka to 1.6-0.8 ka during the

Holocene (preliminary dating results in Vahdati Nasab et al., 2019; full luminescence dating of the Mirak site has now been published, in Heydari et al., 2020).

[Figure 2 about here; in colour]

Material and Methods

Field approach: stratigraphy and sampling strategy

Three series of samples were collected at Mirak N°8 during three missions (2015, 2016, 2017) for sedimentological analysis by the FIPP team. The samples were taken from two sections, here referred to as, respectively, the "northern section" (1 sample/10 centimetres, total of 47 samples) and the "eastern section" (1 sample/5 centimetres, total of 94 samples). The samples from the northern section were referenced by their depth, whereas those from the eastern section are named according to their distance from a specified zero point in the section. In addition, four undisturbed blocks of soil were extracted for micromorphological investigation from the archaeological sections at the boundaries of the stratigraphic units (Fig. 3).

[Figure 3 about here; in colour]

Sedimentological analyses

Grain-size - Grain-size analysis can provide information on transport and sorting of the sediment and hence its genesis (Folk, 1957). The particle size distribution of 141 sediment samples was measured by laser granulometry using a Mastersizer 2000 from MALVERN. The USDA scale (Soil Survey Staff, 2014) was used as our basis for classifying the grain sizes.

Magnetic susceptibility - The use of magnetism to address questions of weathering and pedogenesis patterns, as well as the sources and palaeoenvironmental history of sedimentary records, is well established (Evans and Heller, 2003). In order to obtain a continuous curve of magnetic susceptibility variations along the two sedimentary columns of Mirak N°8, the magnetic susceptibility (κ) of all samples was measured with a Barrington Instruments MS-2 Susceptibility Meter coupled with a MS2B dual frequency sensor. This sensor is generally used to measure the magnetic susceptibility of soil, rock and sediment samples. Low frequency (κ_{lf}, 0.46 kHz) and high frequency (κ_{hf}, 4.6 kHz) were measured three times for each sample in the 0.1 kHz range, to use the average of the three measurements. Only the low frequency results are taken into account and presented in this study.

Calcimetry and quantification of total organic matter - Calcimetry was analysed for the entire record to obtain an understanding of the calcium carbonate variations along the sedimentary columns. The calcium carbonate content of the samples was evaluated through volumetric calcimetry using the Bernard calcimeter method (Duchaufour, 1965; Cailleux and Tricart, 1963). In addition, the loss-on-ignition test was applied, following the standard MA. 1010-PAF 1.0 method (CEAEQ, 2013), to 10 samples from each trench in order to check for the presence or absence of organic matter, and its percentage within the units.

XRD, FTIR and SEM - To complete our knowledge on the mineralogy, nature and pedology of the sediments and to attempt to determine the cause of the anomalies observed in the magnetic

susceptibility data, multiple analyses were implemented using methods such as X-Ray Diffraction (XRD), Fourier transform infrared spectroscopy (FTIR) and scanning electron microscopy (SEM).

- For this purpose, X-ray diffraction was applied to 12 sediment samples from the northern section and 21 sediment samples from the eastern section, using a Bruker XRD (D2) device. The criteria for the selection of these specific samples were based on the importance of their stratigraphic position and the significance of their magnetic susceptibility values. Care was also taken to include at least one representative sample from each designated stratigraphic unit.
- Infrared spectroscopy was carried out as a complementary technique with XRD analysis to determine the nature and composition of certain grains and aggregates encountered during the stereomicroscopic studies. These particles of more or less similar shapes and colours were picked out from the rest of sediments under a stereomicroscope and collected in separate tubes to be analyzed singly, once by XRD analysis and then by FTIR spectroscopy with a Bruker infrared spectrometer.
- 11 particles were picked out from the subsamples during the optical observations for more accurate investigation with a scanning electron microscope (SEM, VEGA/TESCAN). Each particle was micro-photographed and micro-analyzed on multiple points on its surface.

Soil micromorphology and stereomicroscope observation - Micromorphological analysis can contribute to the understanding of past climate and environmental change in arid and semi-arid areas (Stoops et al., 2010). A total of four intact blocks of soil were extracted from the northern section of Mirak N°8 and six thin sections were prepared. However, only four of these were analysed, using the standard Bullock method (1985) and a Zeiss microscope at 4x and 10x magnification under polarized and crossed-polarized light. The original sediments from the same positions selected for XRD analysis in the northern and eastern trenches were nominated this time for optical study, for which the methodology recommended by A. Cailleux (1942) was applied. All three fractions of each sample were studied and micro-photographed using a Zeiss stereomicroscope. The purpose of the optical studies was to investigate the morphology and surface characteristics of the quartz grains (100 to 200 quartz grains per sample) in order to separate them into the two major morphoscopic quartz classes proposed by A. Cailleux (1942): 'blunt shiny' and 'round matt'. The sediments were also analyzed for grain shape, colour, mineralogy, aggregates and any other observable particularity. This classification gave us a clearer knowledge of the source, method of transportation and degree of textural maturity of the majority of the sediments in each stratigraphic unit.

Results

Stratigraphy and sedimentology

The stratigraphic study of the two Mirak N°8 profiles, completed by field observations made on the periphery of the locality, produced a description of 3 main sequences and 10 main units (only

8 of which are visible in the excavation trenches) over the 7-metre thick sequence (Fig. 3). The main characteristics of the various sediments and soil horizons are listed in Table 1. The results of the grain-size and magnetic susceptibility analyses are plotted against the stratigraphy in Figure 4. The grain-size distribution shows a gradually increasing silt fraction (2-50 µm) throughout the lower portion of the eastern section. However, the fine sand fraction (50-200 µm) shows a notable rise in unit 7 and then another less significant increase in unit 5. Above that, the silt curve fluctuates between 45% and 55% up to the top of unit 4b. A comparably decreasing trend appears for the silt fraction in unit 4a. The clay percentage appears to be fairly constant below 12% and fluctuates in parallel with the silt curve throughout the record.

This data shows that Sequence I presents a generally loamy texture according to the USDA soil classification (Fig. 5). However, the grain-size distribution in units 5 and 7 seems to tend further towards the coarser fractions (fine and medium sand) and these two units can therefore be considered as sandy loam. These variations in texture (as reflected in the grain-size curves) point to the role and varying degrees of energy of river systems in transportation and deposition along Sequence I.

The Holocene deposits of Mirak N˚8, here referred to as Sequence II, are made up of six units of aeolian sandy loam (units 3c, 3b, 3a, 2b, 2a, 1). These units are only fully displayed in the northern section, while only the lowermost 0.5m of Sequence II appears in the eastern section. The 3c unit was not sampled for sedimentological analysis.

The $CaCO_3$ percentage curve shows a near-zero value for all units in Sequence I. However, from the topmost part of unit 4a, it starts rising to 20% and appears to be relatively stable all through unit 3b. Most of this $CaCO_3$ is in the form of nodules of the calcareous marl that is frequently found throughout the aeolian sequence. Microscopic observations reject the possibility of an organic origin for these nodules and they were most likely produced by deflation of desert calcrete.

Measurements of total organic matter percentage from 10 representative samples from the various levels of the section showed values from 0.8% to a maximum of 1.4%. This organic matter is mostly composed of vegetal remains and roots and insect excrement.

[Table 1 about here]

Magnetic Susceptibility

Changes in the magnetic susceptibility (MS) values underline major shifts between units in terms of source mineralogy, trace metals and the degree of pedogenesis, and helped to correlate units between the northern and eastern sections. Overall, the MS signal is steadily low in the lowermost 1.5 m of the section (Fig. 4). It shows some weak incremental fluctuations at the base of unit 4b, which subsequently become stronger in unit 4a. The signal then shows a gradually increasing trend up to the top of the record, rising to a maximum of 50.6 κ (10^{-5} S.I.) in Sequence II.

Samples from the two trenches exhibit variations in MS, which displays generally low values indicating only slight pedogenesis in these parts. However, our MS curves show distinct

increases corresponding to the aridisol horizons of Sequence II. As detailed in studies on magnetic properties of wind-blown deposits (e.g. Chlachula et al., 1998; Jia et al., 2012), magnetite and maghemite are the most important magnetic components influencing the magnetic properties of loess/palaeosol sequences. However, concentrations of these minerals may be governed by wind intensity and source mineralogy and not necessarily by the concentration of pedogenic minerals alone.

The 'wind-intensity' mechanism accounts for the fact that during natural windstorms, coarse-grained material contains many more magnetic mineral particles than fine material. As a result, sandy loess deposits transported over a short distance or by strong winds will be characterized by higher magnetic susceptibility values than pure loess (Evans and Heller, 2003; Jia et al., 2012). In this sense, given the widely homogenous mineralogical content, the compositional maturity of the entire record and the higher frequency of sand-sized grains, significantly higher MS results from the aeolian sediments of Mirak N°8 appear to be in closer agreement with the 'wind-intensity' model used to explain a similar feature in the MS record of loess/palaeosol sequences from Siberia (Jia et al., 2012). Nonetheless, extensive aridisol pedogenesis processes could have also been involved in the generation of new magnetic minerals, consequently enhancing low-field magnetic susceptibility in the sediments.

[Figure 4 about here; in colour]

[Figure 5 about here; in colour]

Micromorphology

The main soil micromorphological characteristics of the Mirak N°8 deposits are summarized in Table 2.

Microstructure - Microstructure is generally medium to fine granular or prismatic (only in unit 8), and not well developed (Fig. 6). However, structural development is much more marked in the lower horizons such as in unit 8, while the original structure is disturbed by channels and chambers and biological activity (Fig. 7, B3/E-F) especially in the upper units (e.g., in unit 4a).

Groundmass and b-fabric - The mainly silt-sized groundmass always shows a porphyric relationship with fine to medium sand-sized quartz and soil nodules. The stipple-speckled b-fabric (Fig. 7, B4/G-H) is present in almost all units studied and much more developed in unit 8. The crystallitic b-fabric is a peculiarity of the upper part of unit 4, where weathered carbonate minerals and micritic aggregates are very frequent (Fig. 7, B3/A-B). High percentages of $CaCO_3$ in these levels (Fig. 6) plainly reflect this difference from the lower horizons.

Pedofeatures - Clay and gypsum coatings when present (e.g., in unit 8) are frequent (Fig. 7, B4/A-F). In most other levels, voids are empty or very lightly coated with amorphous Fe/Mn oxide or micrite. In unit 4a the coatings are made up of micrite and the hypocoatings have strongly impregnated the groundmass surrounding the pores, forming a crystallitic b-fabric (Fig. 7, B3/G-H). The frequent presence of pedorelicts (aggregates of soil inherited from the previous stages of soil formation) in the upper parts of unit 4a is noteworthy (Fig. 7, B3/A-B).

Organic material - Woody plant remains, root traces and insect faecal pellets are frequently found within the vesicular pores throughout the setting (Fig. 7, B3/E-F).

[Table 2 about here]

[Figure 6 on a separate landscape page; in black and white]

[Figure 7 on a separate page; in colour]

Morphoscopy of the quartz grains and mineralogy

The main mineralogical components and morphological results are summarized in Figure 6.

Morphoscopy - Morphoscopic analysis of the quartz grains showed that the majority of grains do not meet the criteria for classification into two of the classic morphoscopic categories ("rounded matt" or "angular shiny" quartz grains) identified by A. Cailleux (1942). The "non-worn quartz grains" class covers all the rest of the quartz grains, which have flat polygonal surfaces and show little wear, with a blurry, shiny or intermediate lustre.

Mineralogy - A noteworthy result is the presence of a distinct type of generally sand-sized (0.5 – 1mm) aggregate in some of the horizons within the pedo-sedimentary column, as shown in Figure 8. These structures can be roughly sorted into two types, based on their colour and appearance. Some are brownish yellow to light yellow and some similar structures are very dark to black. Both types are basically ring-like or tubular structures with small empty canals in the middle and are composed of very fine granules supported by a cohesive matrix. SEM microanalysis results state that the granules are fine fragments of quartz and feldspar. The XRD, IFR and SEM results support a mainly clayey composition, consisting of kaolinite, montmorillonite and illite for the matrix of the both types of aggregates.

[Figure 8 about here; in colour]

These aggregates were also found to be rich in the mineral birnessite ($Na_4Mn_{14}O_{27}.9H_2O$) (Fig. 6). It is known that this mineral can form under a variety of physico-chemical conditions and is consequently present in different geological environments such as soils (Taylor et al., 1964; Chukhrov and Gorshkov, 1981; Cornell and Giovanoli, 1988), marine manganese (Mn) nodules and micronodules (Burns, 1976; Glover, 1977; Chukhrov et al., 1978; 1985; 1989; Drits et al., 1985), and Mn-rich ore deposits (Usui and Mita, 1995). Birnessite found in the Mirak N°8 record apparently formed by slow oxidation and crystallization without the intervention of micro-organisms, as a common mineral in desert varnishes under arid and semi-arid conditions. The yellow and dark aggregates (Fig. 8, up-right) show a very similar composition to that of a desert varnish, which invariably consists of birnessite closely intermingled with hematite and large amounts of clay minerals, generally of the illite-montmorillonite type with minor kaolinite. Moreover, FTIR analysis suggests small concentrations of goethite. It thus stands to reason that the tubular structures are in fact the broken remnants of ferruginous surface coatings (pedo-features) that were originally concreted *in situ* around the roots and plant remains in the upper horizons (A or E) of a palaeosol. However, theories on the genesis of ferruginous concretions in soils and weathering profiles are still in debate. In particular, whether the concretions represent

in situ pedogenesis or are transported residues of 'laterite' weathering or ferricrete formation is unclear (e.g. see Löhr et al., 2010).

Discussion

Morpho- and chrono-stratigraphy and pedo-sedimentary evolution

On the basis of the stratigraphic data collected from the two trenches and complemented by observations made laterally on the periphery of the Mirak N°8 mound, it is possible to distinguish three sequences (Fig. 9), each separated from the next by an erosion phase or a significant shift in the sedimentary regime.

[Figure 9 about here; in black and white]

-***Sequence I*** : *alluvial system, with two sub-sequences:*

- *Unit 8 and below: back-swamp environment*. This consists of at least 2-3 m of non-calcareous, very light brown (10 YR 7/3) to green (gley 16/5G) silt loam to silt clay loam with thin interlayers of reddish brown (10YR 4/6) silty clay loam. This basal sequence has a strongly prismatic to blocky structure. OSL dating results suggests 55-44 ka for the top of unit 8, and 73-56 ka for the bottom of this unit (Heydari et al., 2020). Yellow and dark stains of rust and Mn-Fe oxides are ubiquitous and appear to be post-sedimentary in nature. The grain-size distribution curves show a massive drop in the mean size at about 30 cm below the upper limit of sequence I (unit 8). The upper 30 cm appears to be to some extent integrated with younger and coarser sediments and thus represents a more or less similar grain-size frequency distribution to that of the overlying units. However, our grain-size data show a significant increase in the clay content from less than 5% to more than 20%, and of over 40% in the silt content, which means that the oldest deposits (near the bottom of unit 8) of Mirak N°8 are almost entirely composed of silt loam and silty clay loam (Fig. 4). A number of hand-coring samplings carried out at the base of the eastern trench revealed that a texturally similar and more or less homogenous bedding continues for almost 2 metres below the surface until it is almost completely replaced by reddish brown (10YR 4/6) silty clay loam. At a depth of about 2 m, our corings show evidence of a highly carbonated layer (calcrete?) at least 50 cm thick.

- *Units 4 to 7: floodplain environment with evidence of alternating dry and wet seasons*. The larger portion of Sequence I represents the deposition of more than 3 m of mostly loam accumulation (according to the USDA soil classification). It is made up of four stratigraphic units (unit 4 subdivided into 4a and 4b, and units 5, 6 and 7). The entire sequence appears to have been deposited during the Middle Pleniglacial between 55-44 ka to 28-23 ka (Heydari et al., 2020). Based on geomorphology, lithology, grain-size distribution and micromorphology, Sequence I of the Mirak N°8 mound is interpreted as an alluvial sedimentary body deposited in a floodplain environment fed by seasonal currents (flooding events?) running southwards from the southern foothills of the Alborz range. The grain-size distribution shows an overall dominance of silt (2-50 µm) and fine sand (50-200 µm) fractions in approximately 50/50 proportions throughout the sequence (Fig. 4). Yet some intervals within units 7 and 5 show 5-10% increases

in the proportions of coarser fractions such as fine and medium sand. The clay fraction (< 2 µm) remains constant between 6 and 10%, following a very similar trend to that of the silt fraction. The transitional band between units 5 and 6 contains the largest clay fraction (up to 12% clay) in the entire section.

There is evidence for a sedimentary gap and a weathering period between unit 8 and overlying units 7 and 6. Unit 8 is indeed likely to represent the topmost part of a former palaeosol sequence that was later eroded by flood currents and buried under the coarser-grained sandy loam sediments of unit 7 (crevasse splay). The beddings are characterized by pale green silty sand layers, showing current ripples (Sr) and internal planar crossbedding corresponding to the (Sp) lithofacies of Miall (1996). A similar lithofacies is also observed in unit 5. Both units 7 and 5 have embedded Palaeolithic remains and Pleistocene fossils.

Overall, this sequence corresponds to an alluvial system evolving through successive phases of deposition and pedogenesis. The soil/sediment samples represent a generally loam texture according to the USDA soil classification (Fig. 5). However, the grain-size distribution of units 5 and 7 seems to tend more towards the coarser fractions (fine and medium sand), so that these two units can be considered as sandy loam. These variations in texture, reflected in the grain-size curves, confirm the role of fluvial systems with varying degrees of energy in the transportation and deposition of the materials in these units. Given the geomorphological context, fine sedimentation occurred during overbank flooding or distal fluvial spreading from upstream (Alborz mountains). It is characterized by a silty loam facies (units 4 & 6) with a blocky structure.

From a pedological point of view, the build-up of Sequence I can broadly be considered as an alluvial or *cumulic* soil (up-building soil). Our data suggests that during the Upper Pleistocene, continuous deposition under arid climatic conditions left little chance for a mature profile to form. It appears that incipient soil horizons were continually forming with each subsequent flooding event. These widespread, short and shallow floods occurred weekly, monthly or annually in the area. Thus, all of the cumulic soils of the site are basically composed of little-developed sediments and soil nodules. Sequence I is composed of buried A and A-Bw horizons (aridisols) within vertical-accretion flood-plain deposits of silt and clay, with periodic intrusions of higher-velocity currents and deposition of sand splay inter-beddings.

Multiple drainage and desiccation episodes are materialized in the units by the high oxidation and the polyhedral to prismatic structure produced by drastic lowering of the water table. A major phase of desiccation is moreover expressed by the encrusting and crystallization of calcareous nodules at the top of unit 4b. The topmost unit of Sequence I (unit 4a), however, is markedly lighter in colour (5 Y 7/1 to 5 Y 8/1) in comparison to the rest of the sequence which, along with pronounced bioturbation (root holes, wormholes etc.), a high density of Fe-Mn stains and embedded Palaeolithic remains, may represent the depleted zone (reductic horizon) of a palaeosol subsurface. These features are more apparent in the eastern section, which may be due to the lower degree of intermixing with the overlying layers. This silt-loam body corresponds to a hydromorphic horizon, which reflects an episodic phase of waterlogging. This facies (unit 4a) is visible in all the stratigraphic profiles of Mirak N°8. A similar facies pattern was occasionally

observed (in areas where the surface has been incised by water erosion) as far as about 2 km from Mirak N°8. This episode of water saturation is most often followed by a subsequent oxidation phase contemporaneous with the Holocene climatic amelioration. The uppermost limit of unit 4a is irregular and marked by a major unconformity, with an age range of 28-23 ka (Heydari et al., 2020), which indicates extensive deflation of the surface of the *Dasht-e-Kavir* during early MIS 2.

- ***Sequence II*** : *hydromorphic soil complex developed on aeolian deposits (units 1 to 3):*

After a long erosional/non-depositional phase lasting approximately 30 ka, the accumulation of reddish brown aeolian sediments during Holocene began to cover the underlying Pleistocene soil horizons, thus also preserving them from further weathering.

The Holocene deposits of Mirak N°8 start with the deposition of brown calcareous aeolian silts. Sequence II is made up of three units of mostly sandy loam (units 1 to 3, the latter subdivided into 3c, 3b, 3a - 2 -2b, 2a). These units are only fully exposed in the northern section while the eastern section covers only the lowermost 0.5 m of Sequence II. Unit 3c was not sampled for sedimentological analysis.

OSL dating has produced age estimates younger than 0.8-1.6 ka for these deposits (Vahdati Nasab et al., 2019; Heydari et al., 2020). Sequence II therefore overlies the major Pleistocene/Holocene unconformity and is easily distinguishable from the lower layers by its reddish brown colour (7.5 YR 7/4) and coarser texture (mainly sandy loam). The grain-size parameters show an irregular distribution with the fine-sand fraction predominating and strongly fluctuating sorting index values throughout the sequence. A major shift in grain-size distribution occurs at the discontinuity between Sequences I and II. The fine sand fraction rises from around 40% in unit 4 to over 65% in unit 3 while the silt fraction drops to less than 20% (Fig. 4). The medium to coarse sand (200 – 2000 µm) fraction also increases, by 13%, along with the fine sand fraction. The silt and sand fractions fluctuate proportionally by around 10% throughout Sequence II. These fluctuations escalate further up to 20% from the middle of unit 3 to the top of the sequence. These data seem to disagree with the common granulometric pattern of a typical sand dune, which is supposed to be well sorted and increasingly negatively skewed (proportionately more fine-grained material and less coarse-grained material) (Watson, 1989). These definitions are only applicable to the modern sand dune deposits (units 0) that cap the entire mound rather than to the older deposits of Sequence II.

The grain-size distribution, micromorphological results and morphoscopy of the quartz grains of these deposits are characteristic of a nebkha dune. Nebkha dunes, also referred to as nebkhas, shadow dunes, coppices or vegetated dunes, are found commonly throughout the semi-desert regions (e.g. mudflats and flat aeolian fields) of the Middle East (Khalaf et al., 1995; Tsoar and Blumberg, 2002; Saqqa and Atallah, 2004). Nebkhas vary in size and shape depending on wind velocity and wind direction (Worral, 1974; Warren, 1988; Hesp, 1989; Cooke et al., 1993). However, those formed near fluvial channels and mudflat environments usually have a very similar grain-size distribution to that observed in the Mirak N°8 record, with a cohesive combination of silt and clay, less than 50% sand content and small relict soil nodules owing to

aeolian erosion of the surface of the plain (Link et al., 1994; Saqqa and Atallah, 2004; Wang et al., 2006; Ardon et al., 2009). The nebkha hypothesis can also explain the mound-like morphology of the deposits at Mirak N°8.

The desert dust deposits of Sequence II were therefore accumulated some time after the end of the Last Glacial. Iron hydroxide precipitations, calcareous nodules, gypsum crystals and desiccation cracks represent well-marked drying features that are in association with the development of aridisol horizons (Bk, By) (terminology according to Soil Survey Staff, 2014), in an arid environment. Calcium carbonate dominates in sedimentation during the Holocene due to high rates of chemical and biochemical precipitation of calcite and aragonite, especially in summer months (e.g. see Kelts and Shahrabi, 1986). The recurrent lowering of the water table and the increase in evaporative pumping of subsurface moisture through the vadose zone to the surface (Hardie et al., 1978) were the major *in situ* precipitation processes of gypsum and calcareous particles. Holocene desert loess-like depositions must have been formed by frequent dust storms in the deserts that produced much of the silt. Most of the dust was also blown from braided river channels, with a smaller proportion being blown from the desert areas towards the Alborz foothills.

The accumulations of Sequence II would thus be better regarded as series of desert loess-like sediments that have probably been continuously subjected to up-building/ cumulic/ aridisol pedogenesis processes. These unstructured deposits make it possible to formulate the hypothesis of an initial formation of an aeolian mound in an arid context whose development ceased with the establishment of a perched aquifer. The latter marks the development of a minor hydromorphic soil of the stagnosol type (units 1 to 2). Erosional structures resulting from run-off episodes (unit 1) and frost-wedge (reworked blocks) are recognizable in this upper part (Jamet in Berillon et al., 2016). These processes have led to the almost complete disappearance of unit 1 on the northern section and explain the sharp erosion limit between sequence III and sequence II.

- ***Sequence III*** : *peri-desert cover (unit 0):*

Sequence III, observed in the northern section, represents the emplacement of modern calcareous silt deposits of wind-blown origin. This deposit is affected by a slight differentiation in distinct horizons (subunits 0a / 0b / 0c) linked to the development of a young soil. In general, this aeolian cover facies (peri-desert loess-like sediments) is present on the surface of all of the mounds found in the Mirak area.

The widespread and constant presence of needle-like and rounded silicified structures of sponge segments along with fragments of glauconite throughout the Mirak N°8 record is undoubtedly a signal of a sedimentary origin. The nearest geological source of this type of material is reported from the *Mila Formation* in the *Shahmirzad* section about 3 km north of the town of Shahmirzad in Semnan Province, northern Iran (35˚48′40″N, 53˚16′59″E) (Hamdi et al., 1995; Hosseini et al., 2010). Glauconitic sands are also reported in the Neka Valley, Eastern Alborz, Iran (Berra et al., 2007).

Depositional elements and palaeoenvironmental stages

The planar crossbedding lithofacies of unit 7 and the sand loams of unit 5 date back perhaps to the Last Glacial and can be allocated to Marine Isotope Stages (MIS) 3 while chronological correlation of these units remains to be confirmed. The little-developed sandy loam horizon in unit 5 could indicate an environment with higher energy flows. Such soil horizons with pedogenic accumulation of secondary gypsum and other evaporates and Fe/Mn oxides indicate mudflat environments with fluctuations in the ground water level, resulting in periodic submergence of the sediments and subjection to periodic desiccation (Mallol, 2004). The abundance of hydromorphic features in units 7 and 5 reflects an episode of water concentration in the subsurface. Lower temperatures and less evapotranspiration during MIS 3 interstadials in the region (Bobek, 1963; Krinsley, 1970) may have allowed for a more frequent occurrence of overland flows and floods across the piedmont.

Micromorphological and morphological observations have revealed the existence of sub-angular to sub-rounded quartz grains in dominant proportions, associated with sub-rounded feldspars, such as plagioclases (polysynthetic twins) or orthoclase, mica (muscovite), angular fragments of $$weathered chert (microcrystalline SiO_2) and some opaque materials (e.g. iron oxides). Rounded, sub-rounded and prolate gypsum crystals and white fibrous gypsum coatings are a widespread soil component within some zones (see Fig. 8 left) in the record. During drier periods, intense evaporation in semi-arid and arid contexts produced a capillary pressure that sucked up groundwater from the phreatic zone (e.g. the lower part of unit 8) into the vadose zone (e.g. the upper part of unit 8) (Fig. 10), so that lenticular crystals of gypsum were formed from the precipitation of Ca^{2+} and SO^{4-} as coatings in plane voids and channels (Porta, 1990). However, the roundness of authigenic gypsum grains may also be evidence of exposure, desiccation and reworking of the sediments of these units (e.g. see Last and Schweyen, 1985).

[Figure 10 on a separate page; in colour]

Unit 4a exhibits the characteristics of an E horizon. In this unit, voids consist of chambers, channels and compound packing which, in combination with the presence of excrements and plant features (Fig. 7, B3/E-F), can be associated with bioturbation. Almost all of these voids seem empty, with the exception of a few micritic or iron oxide coatings in some channels. The emptiness of the voids indicates eluviation and washing processes (E horizon) as well as the absence of post-depositional illuviation from the overlying horizons. The existence of the reductic horizon of unit 4a, in addition to the scarcity of evaporates and the greatest abundance of ferruginous root coatings, indicate the occurrence of a relatively long period of floodplain stability (stasis) with cold and humid conditions following the cessation of sedimentation into the floodplain basin (from 28-23 ka onwards; Heydari et al., 2020). The absence of gypsum within unit 4a may have also enhanced the preservation of archaeological remains within this particular unit, given the fact that gypsum accumulations have proven to be very damaging to archaeological stratigraphy and materials (Goldberg and Macphail, 2006).

In comparison with the underlying units, unit 3 is characterized by a distinct micritic carbonate matrix (crystallitic microstructure) and little-developed aggregates. Micromorphological observation did not determine any biological indicators and instead showed evidence of intact and weathered detritic carbonate minerals (recognizable by their sharp outline under a polarizing

microscope) and very dominant carbonate impregnations. The origin of detritic carbonates may be calcrete, given the fact that the majority of them are micritic, and sparites are almost non-existent. Soil nodules of relict soil made up of several grains cemented together by calcium carbonates are frequent (Fig. 7, B3/A-B). The integration of this fine carbonated and micritic fraction, combined with the rare occurrence of biological activity, suggests allochthonous contributions linked to deflation processes (wind erosion of calcareous material) in a very arid context (Jamet in Berillon et al., 2016). However, evidence of reworked, dissolved and illuviated carbonates indicates transient wet (relative to modern conditions) episodes.

Archaeological levels

Palaeolithic settlements are more likely to occur in the inactive areas of a floodplain, such as back-swamp or levee, where deposits are coarser and drainage is better. Our results suggest that a low-energy vegetated back-swamp environment under warm climatic conditions was prominent in the area during the formation of the loam soil in unit 8, dated to 55-44 ka (early MIS 3) (Vahdati Nasab et al., 2019; Heydari et al., 2020). It is therefore plausible that the oldest level of the lithic artefacts in the eastern record of Mirak N°8 (L3) was preserved in such an environment, as archaeological materials were buried *in situ* with little post-depositional reworking.

The silt/loam horizons of unit 6, which range in age from 40 to 34 ka (Middle MIS 3) (Heydari et al., 2020) were developed by a very low-energy fluvial system as an anastomosed river which flowed downstream from alluvial fans during a cold and humid period. This period was characterized by slow alluvial aggradation interrupted by rapid flooding events (e.g. the crevasse splay lenses of unit 7) that buried Palaeolithic lithic industries and bones. Crevasse splays are likely to have been briefly occupied by human settlers while active, but would have been more attractive when they became inactive (Goldberg and Macphail, 2006). In addition, the position of these environments continually changed as the channel swept across the floodplain. We therefore suggest that two of the three major Palaeolithic layers of Mirak N°8 (L1 and L2 in Fig. 3 and Fig. 9), owing to very weak sedimentation during a deflation phase, are most probably similar palimpsests resulting from repeated occupations occurring on top of each other. In such situations, sediments and embedded archaeological remains would subsequently be subject to modification and disturbance by post-depositional processes and pedogenesis (displacement by water, bioturbation, physical/chemical weathering, pedoturbation, etc.) until the archaeological pieces were buried and embedded in the sediments of the next shallow flood and preserved from further destruction.

Comparison with other records

A comparison of the Mirak N°8 sequence with other available Quaternary records of the Last Interglacial-Glacial cycle in Eurasia is attempted here. Figure 11 displays correlation lines between the Mirak N°8 sequence and LPS from north-east Iran (Karimi et al., 2009), northern Iran (Kehl et al., 2005; Berillon et al., 2007; Frechen et al., 2009), Armenia (Wolf et al., 2016)

and Central Asia (Frechen and Dodonov, 1998), and with the global marine isotope record (MIS) (Lisiecki and Raymo, 2005).

The OSL age estimates available for the Mirak N°8 sequence seem to concur very well with geological palaeosol records up to 71 ka. Most references from Quaternary palaeoclimatic studies on the Iranian plateau point to alternating dry and cold climatic conditions during the stadials and comparatively moist and warm conditions during the interglacials and interstadials in Iran (Kehl, 2009a). In the loess record for northern Iran, the last interglacial is represented by well-developed Bt forest soil horizons (Kehl et al. 2005). More humid periods during the Quaternary in Iran have also been postulated by Khademi et al. (1997), Khademi and Mermut (1999) and Farpoor et al. (2004), who revealed indicators of higher rainfall rates during MIS 4 than is common today. Although the Mirak N°8 record unfortunately does not cover the Late MIS 5, it is safe to postulate that more water availability for overland flows and higher water-table levels must have been involved in the formation of the lowermost parts in the Mirak N°8 record.

Loess deposits of the late MIS 4 in the Alborz records, such as Toshan and Agh-band (Karimi et al, 2009), are absent in the Mirak N°8 record: this age range is represented instead by moderately pedogenised alluvial deposits that indicate warmer and wetter conditions in central Iran compared to the north during the MIS 4. Old MIS 4 palaeosols (Sequence I) were scoured and buried by the fluvio-alluvial sediments of MIS 3 and 2 until the sedimentary regime shifted to aeolian in MIS 1 and accumulated barely pedogenised desert dusts (Sequence II).

It is likely that two moderately developed Bwk horizons of steppe soils in the loess section at Now Deh (Caspian lowland, northern Iran) correlate with MIS 3 (Frechen et al. 2009). Similar moist and relatively warm conditions during MIS 3 may be presumed at Mirak, when the sandy loam pedo/sediments of unit 5 were formed. There seems to be a considerable chronological gap in the period correlating to MIS 3 and MIS 4 in the records for northern and north-eastern Iran, whereas Mirak's record for MIS 3 shows good stratigraphical consistency with contemporaneous horizons in Central Asia (e.g. Darai Kalon in Tadjikistan). Thus, it may not be too far-fetched to assume that these layers were correspondingly formed and developed under conditions of globally $$low temperatures. In addition, it is known that in very arid regions, increased sediment load in rivers may result from increased rainfall (Tooth, 2000). Based on the above discussion, it can be presumed that the (relatively) fast deposition of the sediments of unit 5 at Mirak N°8 was driven by higher rainfall rates in the region during late MIS 3. Most of this rainfall may generally be attributed to the Northern Hemisphere Westerly Jet climate system, but to what extent and magnitude is difficult to speculate.

Loess accumulated during MIS 2 at Toshan and Agh-band sections suggest a windier and more arid Last Glacial Maximum (LGM) in north-eastern Iran (Karimi et al., 2009; Wang et al., 2016). Such Last Glacial (MIS 2) loess deposits are almost completely lacking at Mirak, which is probably due to a long arid period with no sediment deposition and marked by desiccation and sub-aerial weathering processes.

Lastly, Holocene (MIS 1) dust accumulations at Mirak N°8 lie directly on the MIS 3 alluvial deposits. These successions were most probably subjected to changing water levels and aridisol (Bk, By) pedogenesis processes during the late Holocene dry period (Bobek, 1963), at some stage between c. 9000 and 4000 yrs. BC.

[Figure 11 on a separate landscape page; in black and white]

Conclusion

The archaeological excavations of the Mirak N°8 mound organized from 2015 to 2017 have recorded two sequences, 7m and 5m in length, which document at least the last 50 ka in the dynamic evolution of the sedimentary environment near the central Iranian desert. Our study shows that the mound is structurally made up of three major sedimentary sequences that were formed in two dominant types of environment: alluvial environments with floodplain deposits during the Upper Pleistocene (Sequence I) and sub-desert conditions as indicated by calcareous aeolian nebkha deposits during the Holocene (Sequences II and III).

The alluvial succession is represented by alternating horizons of incipiently pedogenised bodies of loam, inter-stratified with splay sand layers. Our multi-proxy data indicate that these Pleistocene sediments were deposited under moist and warm conditions in a floodplain environment, disturbed periodically by high-energy flooding events. The sediments then dried out and a cracked fine-grained aridisol developed, implying a gradually increasing prevalence of more arid conditions. Middle Palaeolithic prehistoric remains occur exclusively beneath the coarser-grained splay bodies and at the topmost limit of the alluvial sequence, the latter seeming to be palimpsests remaining from recurrent occupations on top of each other in an inactive sedimentary environment. The archaeological levels were then preserved by burial under more recent fluvial or aeolian deposits.

A shift from fluvial succession to coarser-sized aeolian assemblages of calcareous, gypsiferous aridisols (Bk, By) is clearly reflected in the grain-size distribution, magnetic susceptibility and total $CaCO_3$ curves. Chronologically, this shift may have occurred some time during MIS 2, but due to a sedimentation hiatus in the Mirak N°8 record, we are unable to propose a more precise date. There is evidence of a temporal phase of climatic amelioration following the cessation of dust illuviation.

Results from XRD, FTIR, SEM and optical microscopy analyses show near-similar mineralogy for the entire record, regardless of the type of depositional regime. The existence of glauconite, authigenic euhedral quartz crystals and sponge spicules indicate a sedimentary parent rock (e.g. *Mila Formation*), whereas prismatic and only slightly rounded grains of feldspar, diopside, amphibole, etc. may point to a fairly local igneous source rock (e.g. *Karaj Formation*). Therefore, despite the minor differences, the parent rock composition, transportation directions and burial history may have been quite similar for all layers, so that a polygenic source is very likely. Moreover, the high content of unstable minerals, low degree of rounding of the grains, relatively high percentage of clay and silt content and low degree of sorting indicate that the

sediments are compositionally immature. Accordingly, a rather short transportation distance and a local source for the sediments in the record can be presumed.

Lastly, the high aeolian input, the increase in evaporitic minerals, carbonate nodules and aggregates of ferruginous coatings and the change in sediment colour around1.6 ka suggest a shift towards semi-arid and arid conditions in a mudflat environment.

Funding

The fieldwork and geological analyses performed under the joint French and Iranian Palaeoanthropological Program (FIPP) were supported and funded by the office of the Governor of Semnan (Dr. Khabbaz and his deputy Mr. Zandieh Vakil), the French Ministry for European and Foreign Affairs (MEAE) and the CNRS-MNHN-UPVD UMR7194 laboratory (Paris). The luminescence dating study was conducted thanks to financial support from the French National Research Agency via the LaScArBx Labex (Project number ANR-10-LABX-52). This research is conducted as part of a doctoral program at the University of Paris 1 Panthéon-Sorbonne and supported by a doctoral grant from the French Embassy in Iran.

Acknowledgements (to be completed)

We would like to thank the Research Centre for Cultural Heritage and Tourism of Iran (RICHT) and the Iranian Centre for Archaeological Research (ICAR) for granting us permission to conduct the fieldwork at the site, Mr. Jalil Golshan at the RICHT for his support during the 3 seasons of the field missions, the Office of International Affairs at the RICHT for facilitating the visa process for the non-Iranian partners of the project and for exporting the samples studied, and Mr. Khajeh Beidokhti, the director of the Iranian Cultural Heritage Organization (ICHO) office in Semnan Province, and his colleagues for providing ideal conditions to conduct the fieldwork. We are grateful to Mr. Soroush Hashemi and Kamran Shojaee at the ICHO office in Semnan for their logistical support.

The analyses were conducted at the MNHN technical platforms in Paris. We are grateful to our colleagues who provided us with technical support: the XRD analyses were conducted under the supervision of Marie-Madeleine Blanc-Valleron (UMR 5143 CR2P, MNHN, Paris); the FTIR and magnetic susceptibility analyses were carried out under the supervision of Xavier Gallet and Cecile Chapon-Sao respectively (UMR 7194 HNHP, Musée de l'Homme, Paris); SEM analysis was conducted by Sylvain Pont (Institut de Minéralogie, de Physique des Matériaux et de Cosmochimie, MNHN, Paris). We thank Ilona Zaria Bossanyi for language revisions to the final draft of this article.

References

- Ardon, K., Tsoar, H. and Blumberg, D.G., 2009. Dynamics of nebkhas superimposed on a parabolic dune and their effect on the dune dynamics. Journal of Arid Environments, 73(11), pp.1014-1022.
- Bayat, O., Karimzadeh, H., Eghbal, M.K., Karimi, A. and Amundson, R., 2018. Calcic soils as indicators of profound Quaternary climate change in eastern Isfahan, Iran. Geoderma, 315, pp.220-230.

- Bayat, N., Rastegar, E., Salvati, L., Darabi, H., Fard, N.A. and Taji, M., 2019. Motivation-based Market Segmentation in Rural Tourism: the Case of Sámán, Iran. Almatourism-Journal of Tourism, Culture and Territorial Development, 10(19), pp.1-24.
- Berillon, G., Khaneghah, A.A., Antoine, P., Bahain, J.J., Chevrier, B., Zeitoun, V., Aminzadeh, N., Beheshti, M., Chanzanagh, H.E. and Nochadi, S., 2007. Discovery of new open-air Paleolithic localities in Central Alborz, Northern Iran. Journal of human evolution, 52(4), pp.380-387.
- Berillon, G., Vahdati Nasab, H. and Asgari Khaneghah, A. (2016). Programme Paléoanthropologique Franco-Iranien - FIPP - 10ème Campagne : Octobre-Novembre 2016 Fouille du site Mirak 8 (unpublished report).
- Berillon, G., Vahdati Nasab, H. and Asgari Khaneghah, A. (2015). Programme Paléoanthropologique Franco-Iranien - FIPP - 9ème Campagne : Juin-Juillet 2015 Fouille du site Mirak 8 (unpublished report).
- Berillon, G., Vahdati Nasab, H. and Asgari Khaneghah, A. (2017). Programme Paléoanthropologique Franco-Iranien - FIPP - 11ème Campagne : Octobre-Novembre 2017 Fouille du site Mirak 8 (unpublished report).
- Berra, F., Zanchi, A., Mattei, M. and Nawab, A., 2007. Late Cretaceous transgression on a Cimmerian high (Neka Valley, Eastern Alborz, Iran): A geodynamic event recorded by glauconitic sands. Sedimentary Geology, 199(3-4), pp.189-204.
- Bobek, H., 1963. Nature and implications of Quaternary climatic changes in Iran.
- Bogemans, F., Janssens, R. and Baeteman, C., 2017. Depositional evolution of the Lower Khuzestan plain (SW Iran) since the end of the Late Pleistocene. Quaternary Science Reviews, 171, pp.154-165.
- Bottema, S., 1986. A late Quaternary pollen diagram from Lake Urmia (northwestern Iran). Review of palaeobotany and palynology, 47(3-4), pp.241-261.
- Bullock, P., Fedoroff, N., Jongerius, A., Stoops, G. and Tursina, T., 1985. Handbook for soil thin section description. Waine Research.
- Burns, R.G., 1976. The uptake of cobalt into ferromanganese nodules, soils, and synthetic manganese (IV) oxides. Geochimica et Cosmochimica Acta, 40(1), pp.95-102.
- Cailleux, A. and Tricart, J., 1963. Initiation à l'étude des sables et des galets (Vol. 1). Centre de documentation universitaire.
- Cailleux, A., 1942. Les actions éoliennes périglaciaires en Europe (Vol. 21, No. 46). Société géologique.
- CEAEQ, 2003. Determination de la matiere organique par incineration : Methode de perte de feu (PAF), MA. 1010 e PAF 1.0. Centre d'Expertise en Analyse Environnementale du Quebec, Quebec, QC, Canada, p. 9. CEAEQ, 2011. Determination des dibenzo-para-dioxines.
- Chlachula, J., Evans, M.E. and Rutter, N.W., 1998. A magnetic investigation of a Late Quaternary loess/palaeosol record in Siberia. Geophysical Journal International, 132(1), pp.128-132.

- Chukhrov, F.V. and Gorshkov, A.I., 1981. Iron and manganese oxide minerals in soils. Earth and Environmental Science Transactions of The Royal Society of Edinburgh, 72(3), pp.195-200.
- Chukhrov, F.V., 1978. Sulfur-isotope phytogeochemistry. Geochem. Intern., 1978, pp.25-40.
- Chukhrov, F.V., Sakharov, B.A., Gorshkov, A.I., Drits, V.A. and Dikov, Y.P., 1985. Crystal structure of birnessite from the Pacific Ocean. International Geology Review, 27(9), pp.1082-1088.
- Chukhrov, F.V., Gorshkov, A.I., Sivtsov, A.V., Berezovskaya, V.V., Dikov, Y.P., Dubinina, G.A. and Varinov, N.N., 1989. Akhtenskite—the natural analog of ε-MnO2. International Geology Review, 31(10), pp.1068-1072.
- Cooke, R., Warren, A., Goudie, A., 1993. Desert Geomor- phology. UCL Press Limited, University College London, London.
- Cornell, R.M. and Giovanoli, R., 1988. Transformation of hausmannite into birnessite in alkaline media. Clays and Clay Minerals, 36(3), pp.249-257.
- Djamali, M., De Beaulieu, J.L., Miller, N.F., Andrieu-Ponel, V., Ponel, P., Lak, R., Sadeddin, N., Akhani, H. and Fazeli, H., 2009. Vegetation history of the SE section of the Zagros Mountains during the last five millennia; a pollen record from the Maharlou Lake, Fars Province, Iran. Vegetation History and Archaeobotany, 18(2), pp.123-136.
- Djamali, M., de Beaulieu, J.L., Shah-hosseini, M., Andrieu-Ponel, V., Ponel, P., Amini, A., Akhani, H., Leroy, S.A., Stevens, L., Lahijani, H. and Brewer, S., 2008. A late Pleistocene long pollen record from Lake Urmia, NW Iran. Quaternary Research, 69(3), pp.413-420.
- Drits, M.E., 1985. Properties of elements: Handbook. Metallurgiya, Moscow, p.672.
- Duchaufour, P., 1965. Precis de Pedologie. Soil Science, 100(1), p.75.
- Evans, M. and Heller, F., 2003. Environmental magnetism: principles and applications of enviromagnetics (Vol. 86). Academic press.
- Folk, R.L. and Ward, W.C., 1957. Brazos River bar: a study in the significance of grain size parameters. Journal of Sedimentary Research, 27 ,.1)pp.3-26
- Frechen, M. and Dodonov, A.E., 1998. Loess chronology of the Middle and Upper Pleistocene in Tadjikistan. Geologische Rundschau, 87(1), pp.2-20.
- Frechen, M., Kehl, M., Rolf, C., Sarvati, R. and Skowronek, A., 2009. Loess chronology of the Caspian lowland in northern Iran. Quaternary International, 198(1-2), pp.220-233.
- Goldberg, P. and Macphail, R., 2006. Practical and theoretical geoarcheology. Malden, Mass.: Blackwell, pp.11 - 150.
- Griffiths, H.I., Schwalb, A. and Stevens, L.R., 2001. Environmental change in southwestern Iran: the Holocene ostracod fauna of Lake Mirabad. The Holocene, 11(6), pp.757-764.
- Glover, E.D., 1977. Characterization of a marine birnessite. American Mineralogist, 62(3-4), pp.278-285.

- Hamdi, B., Rozanov, A.Y. and Zhuravle, A.Y., 1995. Latest Middle Cambrian metazoan reef from northern Iran. Geological Magazine, 132(4), pp.367-373.
- Hamzeh, M.A., Gharaie, M.H.M., Lahijani, H.A.K., Djamali, M., Harami, R.M. and Beni, A.N., 2016. Holocene hydrological changes in SE Iran, a key region between Indian summer monsoon and Mediterranean winter precipitation zones, as revealed from a lacustrine sequence from Lake Hamoun. Quaternary International, 408, pp.25-39.
- Hardie, L.A., Smoot, J.P. and Eugster, H.P., 1978. Saline lakes and their deposits: a sedimentological approach. In Modern and ancient lake sediments (Vol. 2, pp. 7-41). Oxford: Blackwell Scientific Publications.
- Haddadan, M., Afsharian Zadeh, A.M., Chaichi, Z., 1994. Geological quadrangle map of Iran NO. G5., Geological Survey of Iran.
- Hesp, P.A., 1989. A review of biological and geomorphological processes involved in the initiation and development of incipient foredunes. Proceedings of the Royal Society of Edinburgh, Section B: Biological Sciences, 96, pp.181-201.
- Heydari, M., Guérin, G., Kreutzer, S., Jamet, G., Kharazian, M.A., Hashemi, M., Nasab, H.V. and Berillon, G., 2020. Do bayesian methods lead to more precise chronologies?'BayLum'and a first OSL-based chronology for the palaeolithic open-air site of Mirak (Iran). Quaternary Geochronology, p.101082.
- Hosseini, H.K., Lasemi, Y. and Jahani, D., 2010. Depositional environment and sequence stratigraphy of the members 3, 4 and 5 of the Mila Formation in the Hasanak-dar, Central Alborz. In The 1st International Applied Geological Congress, Department of Geology, Islamic Azad University–Mashad Branch, Iran, 26–28 April 2010 (pp. 1522-1527).
- Jia, J., Xia, D., Wang, B., Wei, H. and Liu, X., 2012. Magnetic investigation of Late Quaternary loess deposition, Ili area, China. Quaternary international, 250, pp.84-92.
- Karimi, A., Khademi, H., Kehl, M. and Jalalian, A., 2009. Distribution, lithology and provenance of peridesert loess deposits in northeastern Iran. Geoderma, 148(3), pp.241-250.
- Kehl, M. and Frechen, M. and Skowronek, A., 2008. Zur Pedostratigraphie nordiranischer Lösse. – In: Abh. Geol. B.-A. 62, 158-163
- Kehl, M., 2009a. Quaternary climate change in Iran—the state of knowledge. Erdkunde, pp.1-17.
- Kehl, M., Frechen, M. and Skowronek, A., 2009b. Nature and age of Late Quaternary basin fill deposits in the Basin of Persepolis/Southern Iran. Quaternary International, 196(1-2), pp.57-70.
- Kehl, M., Sarvati, R., Ahmadi, H., Frechen, M. and Skowronek, A., 2005. Loess paleosoil-sequences along a climatic gradient in Northern Iran. E&G Quaternary Science Journal, 55(1), pp.149-173.
- Kelts, K. and Shahrabi, M., 1986. Holocene sedimentology of hypersaline Lake Urmia, northwestern Iran. Palaeogeography, Palaeoclimatology, Palaeoecology, 54(1-4), pp.105-130.

- Khalaf, F.I., Misak, R. and Al-Dousari, A., 1995. Sedimentological and morphological characteristics of some nabkha deposits in the northern coastal plain of Kuwait, Arabia. Journal of Arid Environments, 29(3), pp.267-292.
- Krinsley, D.B., 1970. A Geomorphological and Paleoclimatological Study of the Playas of Iran. Part I. Geological Survey Reston Va.
- Lambert, N.F., 2010. A multiproxy high resolution paleoclimate study of Lake Mirabad, Iran. California State University, Long Beach.
- Lateef, A.S.A., 1988. Distribution, provenance, age and paleoclimatic record of the loess in Central North Iran. Loess-Its Distribution, Geology and Soil. Rotterdam, Balkema, pp.93-101.
- Lauer, T., Vlaminck, S., Frechen, M., Rolf, C., Kehl, M., Sharifi, J., Lehndorff, E. and Khormali, F., 2017. The Agh Band loess-palaeosol sequence–A terrestrial archive for climatic shifts during the last and penultimate glacial–interglacial cycles in a semiarid region in northern Iran. Quaternary international, 429, pp.13-30.
- Last, W.M. and Schweyen, T.H., 1985. Late Holocene history of Waldsea Lake, Saskatchewan, Canada. Quaternary Research, 24(2), pp.219-234.
- Leroy, S.A., Kakroodi, A.A., Kroonenberg, S., Lahijani, H.K., Alimohammadian, H. and Nigarov, A., 2013. Holocene vegetation history and sea level changes in the SE corner of the Caspian Sea: relevance to SW Asia climate. Quaternary Science Reviews, 70, pp.28-47.
- Link, S.O., Waugh, W.J., Downs, J.L., Thiede, M.E., Chatters, J.C. and Gee, G.W., 1994. Effects of coppice dune topography and vegetation on soil water dynamics in a cold-desert ecosystem. Journal of Arid Environments, 27(3), pp.265-278.
- Lisiecki, L.E. and Raymo, M.E., 2005. A Pliocene-Pleistocene stack of 57 globally distributed benthic δ18O records. Paleoceanography, 20(1).
- Löhr, S.C., Grigorescu, M. and Cox, M.E., 2010. Genesis of the ferruginous concretion in a ferric soil and implications for past and present iron mobility. In 19th World Congress of Soil Science, Soil Solutions for a Changing World, Brisbane.
- Mallol, C., 2004. Micromorphological observations from the archeological sediments of Ubeidiya (Israel), Dmanisi (Georgia) and Gran Dolina-TD10 (Spain) for the reconstruction of hominid occupation contexts, PhD Thesis, Harvard University, Cambridge, United States.
- Mehterian, S., Pourmand, A., Sharifi, A., Lahijani, H.A., Naderi, M. and Swart, P.K., 2017. Speleothem records of glacial/interglacial climate from Iran forewarn of future Water Availability in the interior of the Middle East. Quaternary Science Reviews, 164, pp.187-198.
- Miall, A.D., 1996. The Geology of Fluvial Deposits: Sedimentary Facies, Basin Analysis. Petroleum Geology. Springer-Verlag, New York, p.582.

- Pickarski, N., Kwiecien, O., Langgut, D. and Litt, T., 2015. Abrupt climate and vegetation variability of eastern Anatolia during the last glacial. Climate of the Past, 11(11), pp.1491-1505.
- Porta, J. and Herrero, J., 1990. Micromorphology and genesis of soils enriched with gypsum. Developments in Soil Science, 19, pp.321-339.
- Ramezani, E., Marvie Mohadjer, M.R., Knapp, H.D., Ahmadi, H. and Joosten, H., 2008. The late-Holocene vegetation history of the Central Caspian (Hyrcanian) forests of northern Iran. The Holocene, 18(2), pp.307-321.
- Regard, V., Bellier, O., Braucher, R., Gasse, F., Bourlès, D., Mercier, J., Thomas, J.C., Abbassi, M.R., Shabanian, E. and Soleymani, S., 2006. 10Be dating of alluvial deposits from Southeastern Iran (the Hormoz Strait area). Palaeogeography, Palaeoclimatology, Palaeoecology, 242(1-2), pp.36-53.
- Rezvani, H. and Vahdati Nasab, H., 2010. A Major Middle Palaeolithic Open-air Site at Mirak, Semnan Province, Iran. Antiquity, 84(323), Project Gallery.
- Rezvani, H., 1990. Settlement patterns of prehistoric cultures in Semnan, in A. Alizadeh, Y. Majidzadeh & S. Malek Shahmirzadi (ed.) The Iranian world. Essays on Iranian art and archeology presented to Ezat O. Negahban: 7-19. Tehran: Iran University Press (papers in English or Iranian with summaries).
- Saqqa, W. and Atallah, M., 2004. Characterization of the aeolian terrain facies in Wadi Araba Desert, southwestern Jordan. Geomorphology, 62(1-2), pp.63-87.
- Sharifi, A., Pourmand, A., Canuel, E.A., Ferer-Tyler, E., Peterson, L.C., Aichner, B., Feakins, S.J., Daryaee, T., Djamali, M., Beni, A.N. and Lahijani, H.A., 2015. Abrupt climate variability since the last deglaciation based on a high-resolution, multi-proxy peat record from NW Iran: The hand that rocked the Cradle of Civilization?. Quaternary Science Reviews, 123, pp.215-230.
- Shoaee, M.J., Nasab, H.V. and Petraglia, M.D., 2021. The Paleolithic of the Iranian Plateau: Hominin occupation history and implications for human dispersals across southern Asia. Journal of Anthropological Archeology, 62, p.101292.
- Soil Survey Staff, 2014. Keys to Soil Taxonomy, 12th ed. USDA-Natural Resources Conservation Service, Washington, DC.
- Stevens, L.R., Wright Jr, H.E. and Ito, E., 2001. Proposed changes in seasonality of climate during the Lateglacial and Holocene at Lake Zeribar, Iran. The Holocene, 11(6), pp.747-755.
- Stevens, L.R., Ito, E., Schwalb, A. and Wright Jr, H.E., 2006. Timing of atmospheric precipitation in the Zagros Mountains inferred from a multi-proxy record from Lake Mirabad, Iran. Quaternary research, 66(3), pp.494-500.
- Taheri, M., Khormali, F., Wang, X., Amini, A., Wei, H., Kehl, M., Frechen, M. and Chen, F., 2017. Micromorphology of the lower Pleistocene loess in the Iranian Loess Plateau and its paleoclimatic implications. Quaternary International, 429, pp.31-40.

- Taylor, R.M., McKenzie, R.M. and Norrish, K., 1964. The mineralogy and chemistry of manganese in some Australian soils. Soil Research, 2(2), pp.235-248.
- Thomas, D.S., Bateman, M.D., Mehrshahi, D. and O'hara, S.L., 1997. Development and environmental significance of an eolian sand ramp of last-glacial age, Central Iran. Quaternary Research, 48(2), pp.155-161.
- Tooth, S., 2000. Process, form and change in dryland rivers: a review of recent research. Earth-Science Reviews, 51(1), pp.67-107.
- Tsoar, H. and Blumberg, D.G., 2002. Formation of parabolic dunes from barchan and transverse dunes along Israel's Mediterranean coast. Earth Surface Processes and Landforms, 27(11), pp.1147-1161.
- Usui, A. and Mita, N., 1995. Geochemistry and mineralogy of a modern buserite deposit from a hot spring in Hokkaido, Japan. Clays and Clay Minerals, 43(1), pp.116-127.
- Vaezi, A., Ghazban, F., Tavakoli, V., Routh, J., Beni, A.N., Bianchi, T.S., Curtis, J.H. and Kylin, H., 2019. A Late Pleistocene-Holocene multi-proxy record of climate variability in the Jazmurian playa, southeastern Iran. Palaeogeography, palaeoclimatology, palaeoecology, 514, pp.754-767.
- Vahdati Nasab, H., 2009. The Palaeolithic survey of Mirak. Unpublished report prepared for the Iranian Center for Archeological Research, Iranian Cultural Heritage and Tourism Organization (in Persian).
- Vahdati Nasab, H., Berillon, G., Jamet, G., Hashemi, M., Jayez, M., Somaye, K., Anvari, Z., Guérin, G., Heydari, M., Akhavan Kharazian, M., Puaud S., Bonilauri, S., Zeitoun, V., Sévêque, N., Darvishi Khatooni, J., Asgari Khaneghah, A., 2019. The Open-Air Paleolithic Site of Mirak, Northern Edge of the Iranian Central Desert (Semnan, IRAN): Evidence of repeated human occupations during the late Pleistocene. Comptes rendus Palevol, 18(4), pp.465-478.
- Vahdati Nasab, H., Clark, G.A. and Torkamandi, S., 2013. Late Pleistocene dispersal corridors across the Iranian Plateau: a case study from Mirak, a Middle Paleolithic site on the northern edge of the Iranian Central Desert (Dasht-e Kavir). Quaternary international, 300, pp.267-281.
- Van Zeist, W. and Wright, H.E., 1963. Preliminary pollen studies at Lake Zeribar, Zagros mountains, southwestern Iran. Science, 140(3562), pp.65-67.
- Van Zeist, W., 1991. Late Quaternary vegetation of the Near East. Beihefte zum Tubinger Atlas des Vorderen Orients. Reihe A, 18, pp.1-156.
- Vlaminck, S., Kehl, M., Rolf, C., Franz, S.O., Lauer, T., Lehndorff, E., Frechen, M. and Khormali, F., 2018. Late Pleistocene dust dynamics and pedogenesis in Southern Eurasia–Detailed insights from the loess profile Toshan (NE Iran). Quaternary Science Reviews, 180, pp.75-95.
- Wang, X., Wang, T., Dong, Z., Liu, X. and Qian, G., 2006. Nebkha development and its significance to wind erosion and land degradation in semi-arid northern China. Journal of Arid Environments, 65(1), pp.129-141.

- Wang, X., Wei, H., Taheri, M., Khormali, F., Danukalova, G. and Chen, F., 2016. Early Pleistocene climate in western arid central Asia inferred from loess-palaeosol sequences. Scientific Reports, 6(1), pp.1-9.
- Warren, A. and Agnew, C., 1988. An assessment of desertification and land degradation in arid and semi-arid areas (No. 2). International Institute for Environment and Development.
- Wasylikowa, K., Witkowski, A., Walanus, A., Hutorowicz, A., Alexandrowicz, S.W. and Langer, J.J., 2006. Palaeolimnology of Lake Zeribar, Iran, and its climatic implications. Quaternary Research, 66(3), pp.477-493.
- Watson, A., 1989. Windflow characteristics and aeolian entrainment. Arid zone geomorphology, pp.209-231.
- Weise, O.R. and OR, W., 1974. Zur Hangentwicklung und Flächenbildung im Trockengebiet des iranischen Hochlandes. Würzburger Geogr. Arb. 42. Würzburg

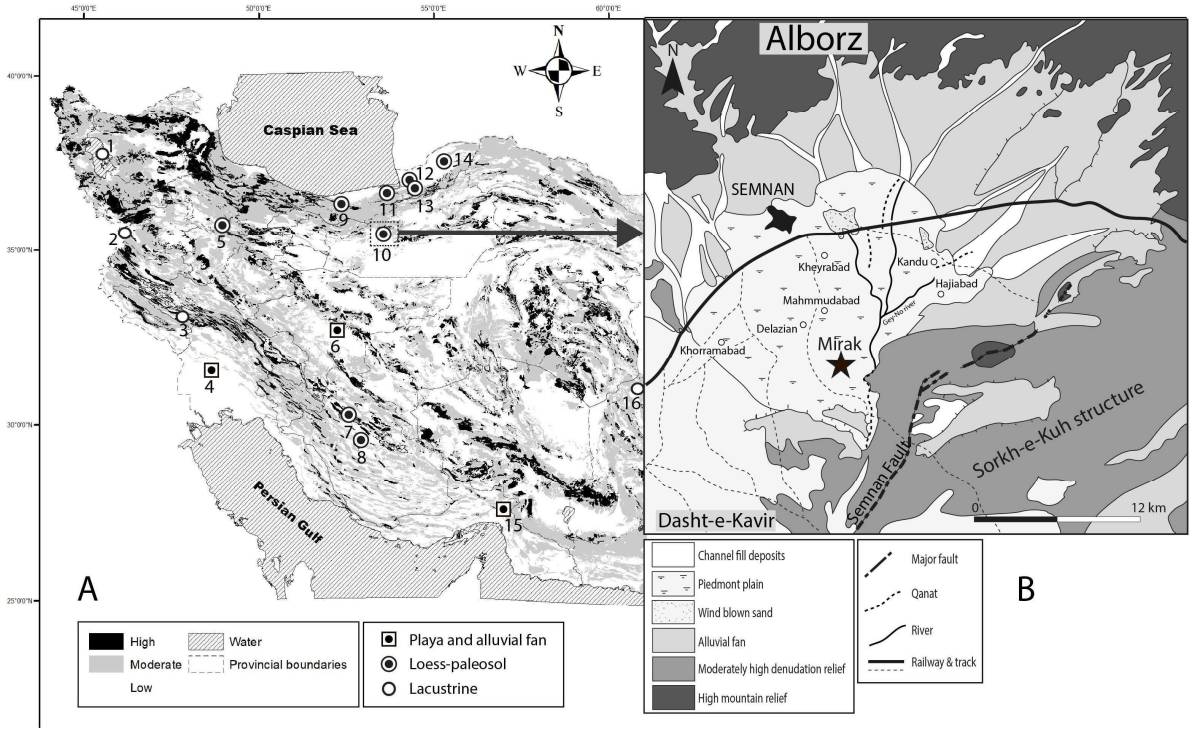

- Figure 1 Map of some of the major quaternary palaeoclimatic sites studied in Iran:

1. Lake Urmia (Djamali et al., 2008)
2. Lake Zeribar (Stevens et al., 2006)
3. Lake Mirabad (Lambert, 2010)
4. Khuzestan plain (Bogemans, 2017)
5. Qaleh Kord cave (Mehterian et al., 2017)
6. Eastern Esfahan (Bayat et al., 2018)
7. Persepolis Basin (Kehl et al., 2009b)
8. Lake Neyriz (Krinsley, 1970)
9. Garm Roud (Berillon et al., 2007)
10. Mirak mound (the present study)
11. Neka (Kehl et al., 2008)

12,13. Toshan & No deh (Vlaminck et al., 2018)

14. Agh band (Wang et al., 2016)
15. Hormoz strait area (Regard et al., 2006)
16. Lake Hamoun (Hamzeh et al. 2016)

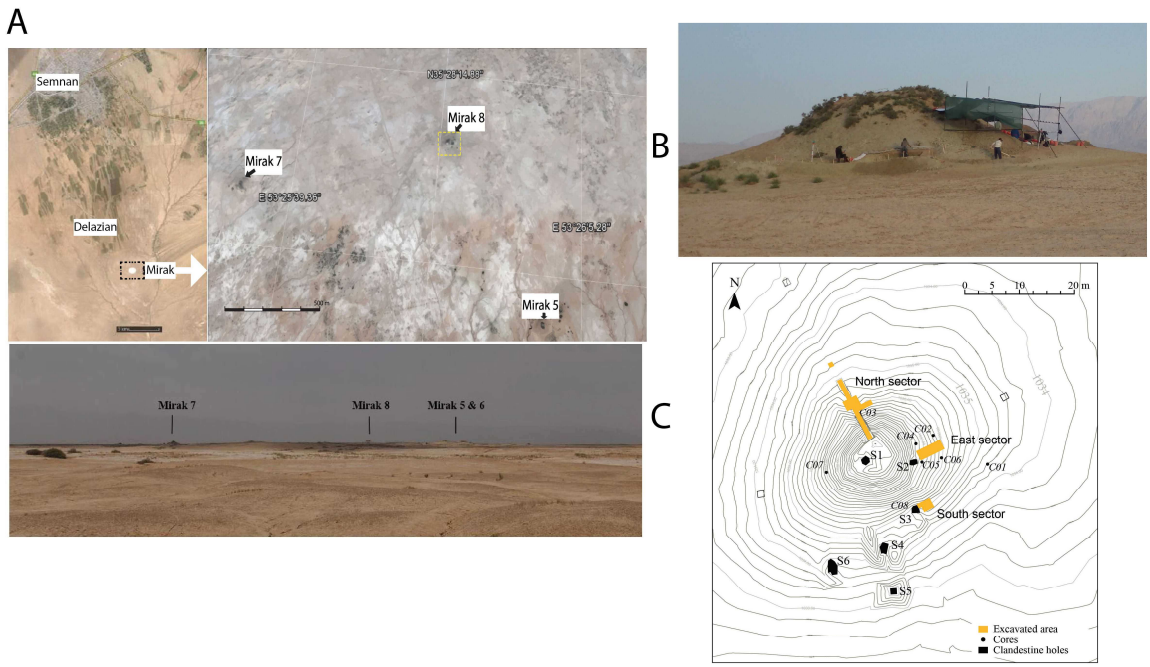

- Figure 2 A: Satellite image of the location of the mounds in Mirak; and B: Mound number 8 at Mirak. C: Topography of Mirak N°8 and location of archaeological trenches at the site.

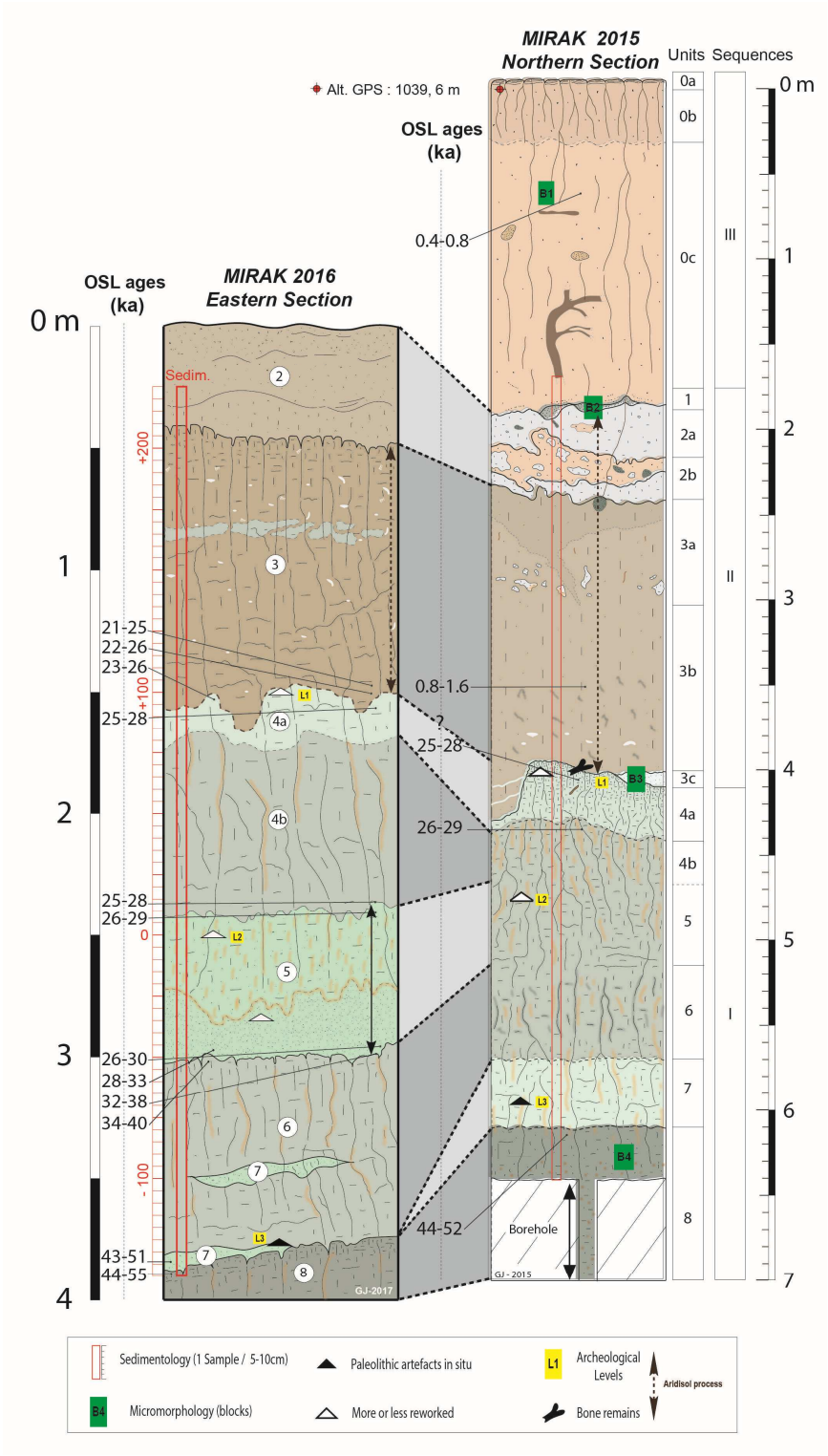

- Figure 3 Stratigraphic profiles of the northern and eastern sections. The two columns are correlated on the basis of pedostratigraphy (modified from sedim. logs made by Guillaume Jamet, in Berillon et al., 2016). The ages presented here are Bayesian OSL ages from Heydari et al., 2020.

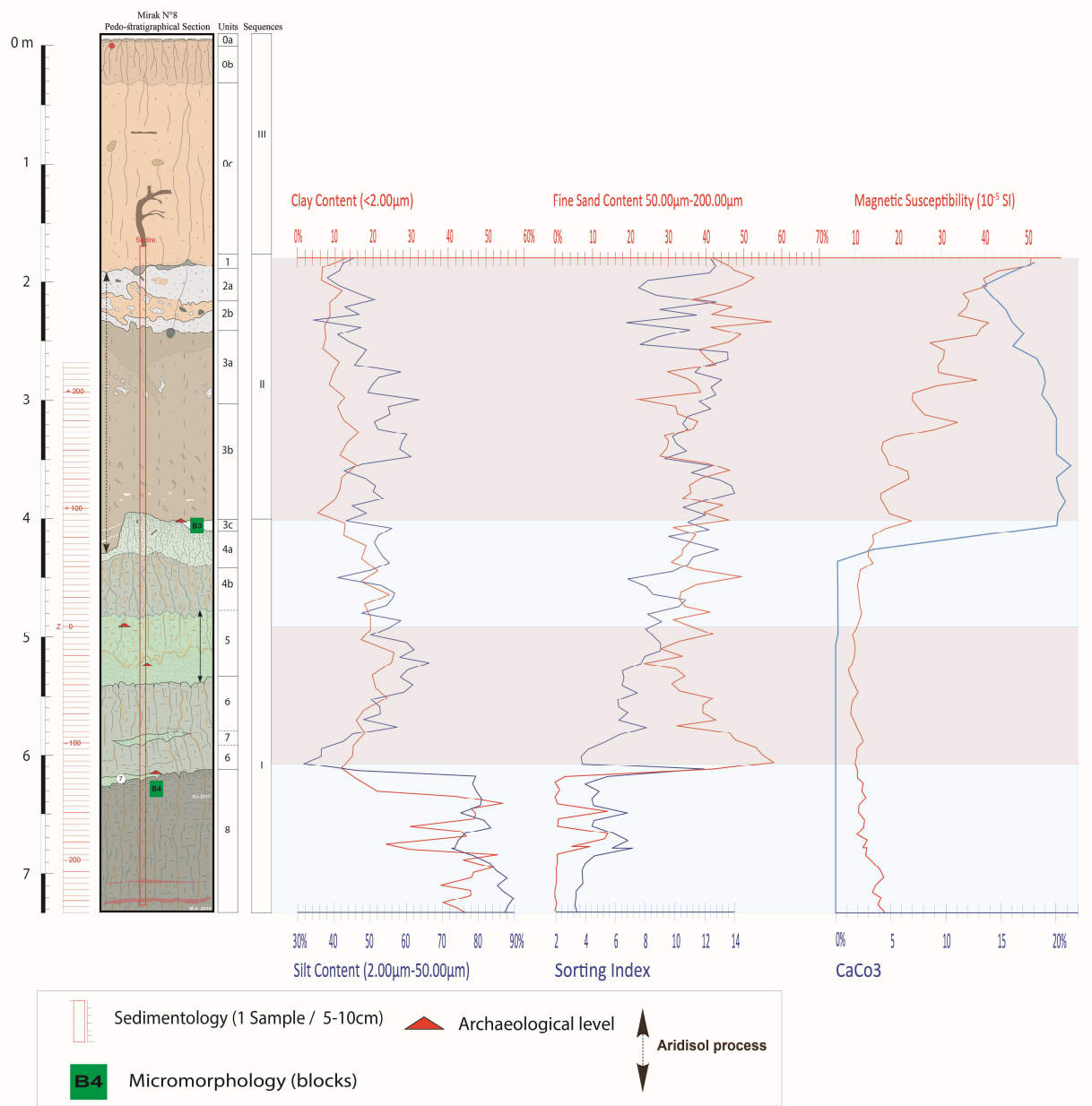

- Figure 4 All granulometric and MS datasets plotted against the sedimentary column. Clay = 0.01 - 2 µm. Silt = 2 - 50 µm. Fine Sand= 50 - 200 µm. Medium to Coarse Sand = 200 - 500 µm. Sorting index = d(0.75)/d(0.25)

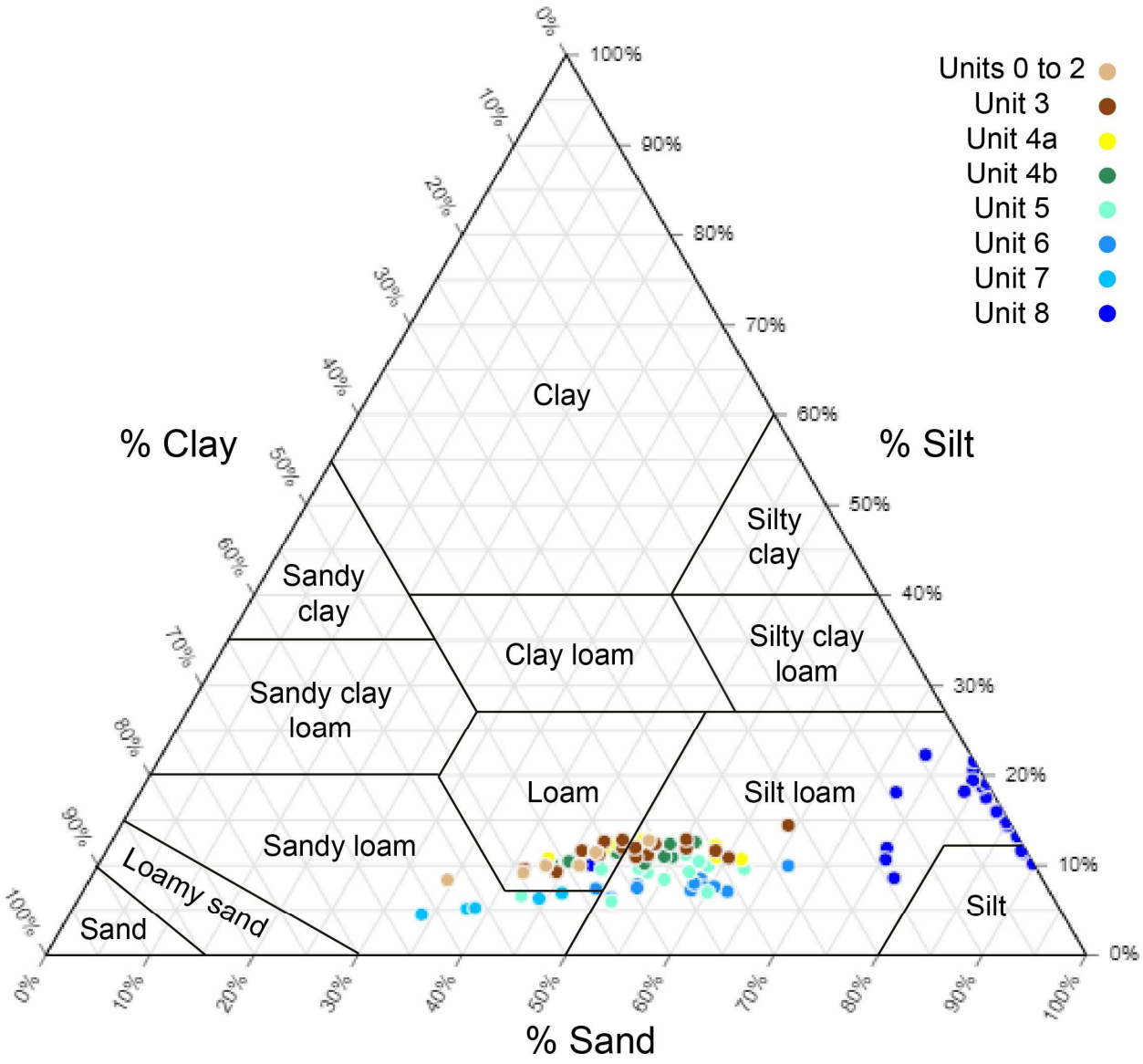

Figure 5 Ternary diagram of the soil texture triangle showing the different USDA-based soil texture classifications and texture of sediment samples from different stratigraphic units of Mirak N°8.

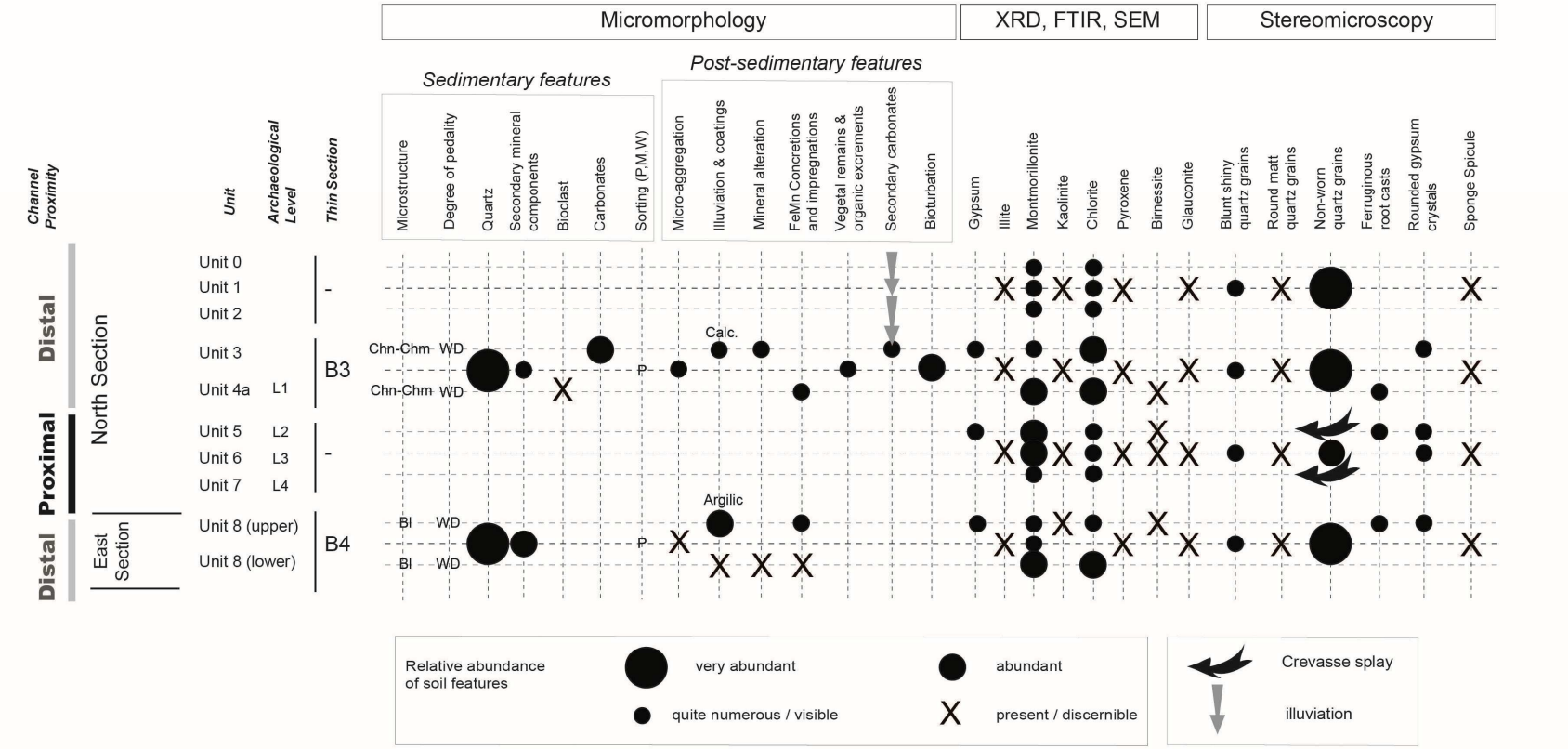

- Figure 6 Summary of micromorphological, mineralogical and stereomicroscopic analyses results, Mirak N°8. Chn-Chm: Channel and chamber, Bl: Blocky, WD: Well developed, P: Poor

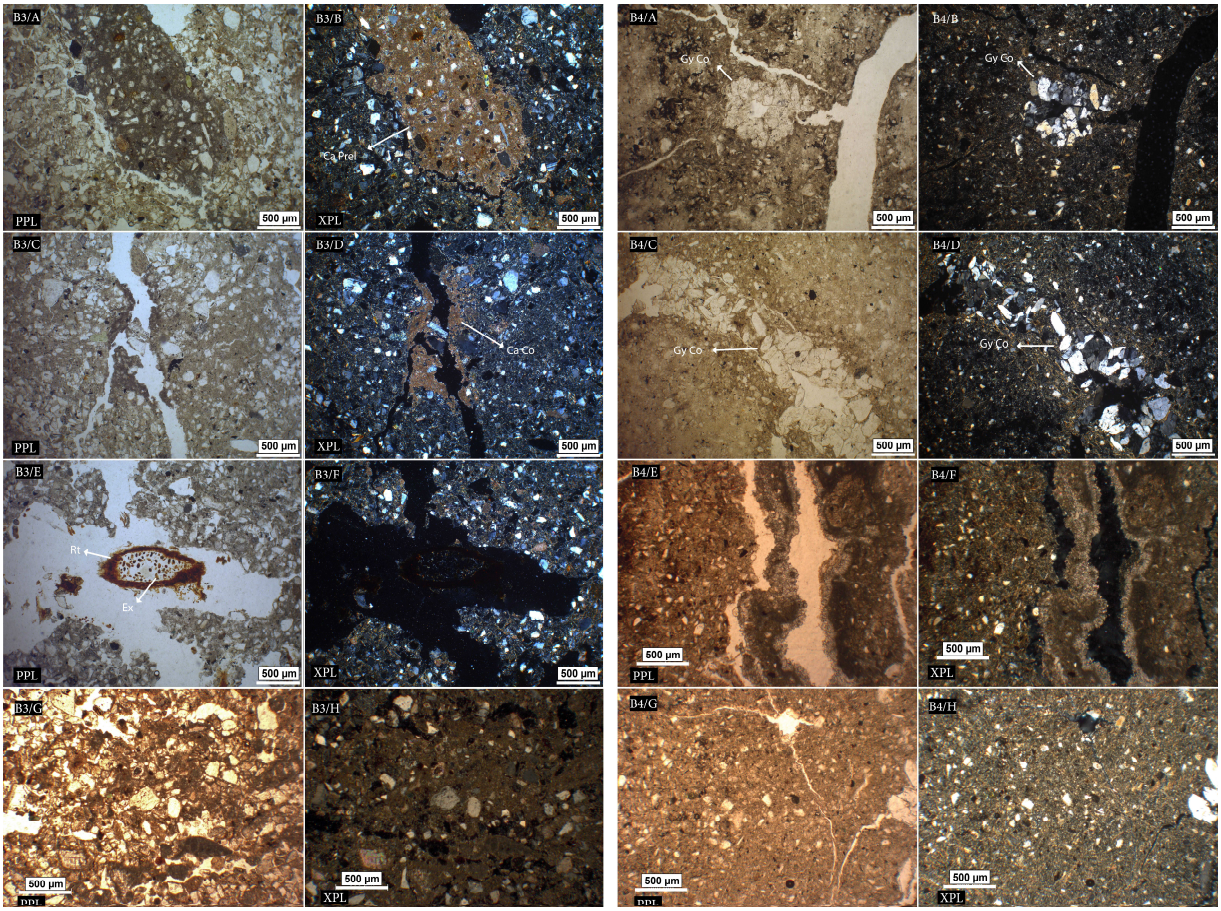

- Figure 7 soil micromorphology of the northern section of Mirak N° 8. Ca: carbonate; Prel: pedorelict; Co: coating; Rt: roots; Ex: faecal pellets; Gy: gypsum.

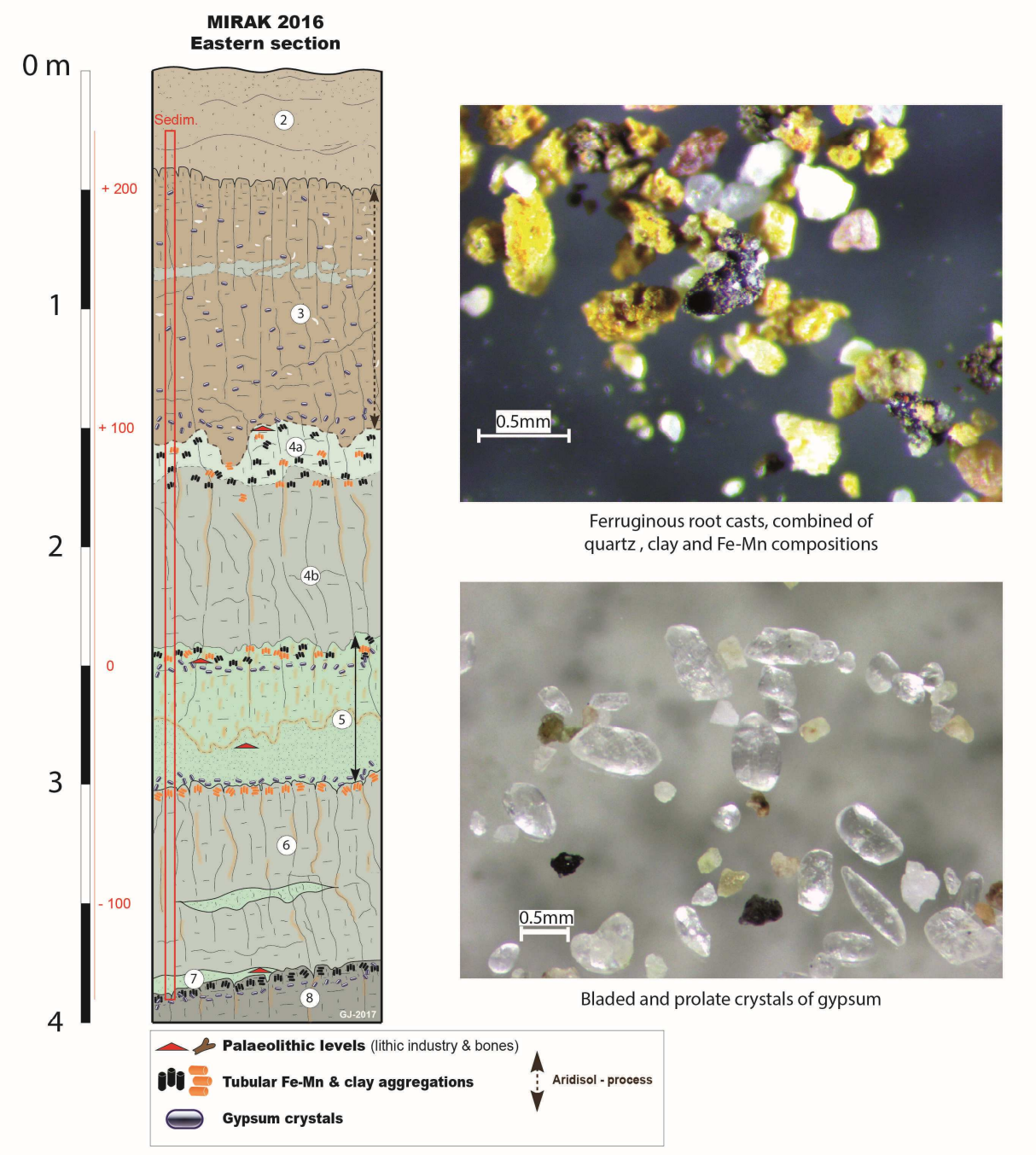

- Figure 8 Stratigraphic position of ferruginous aggregates and gypsum crystals

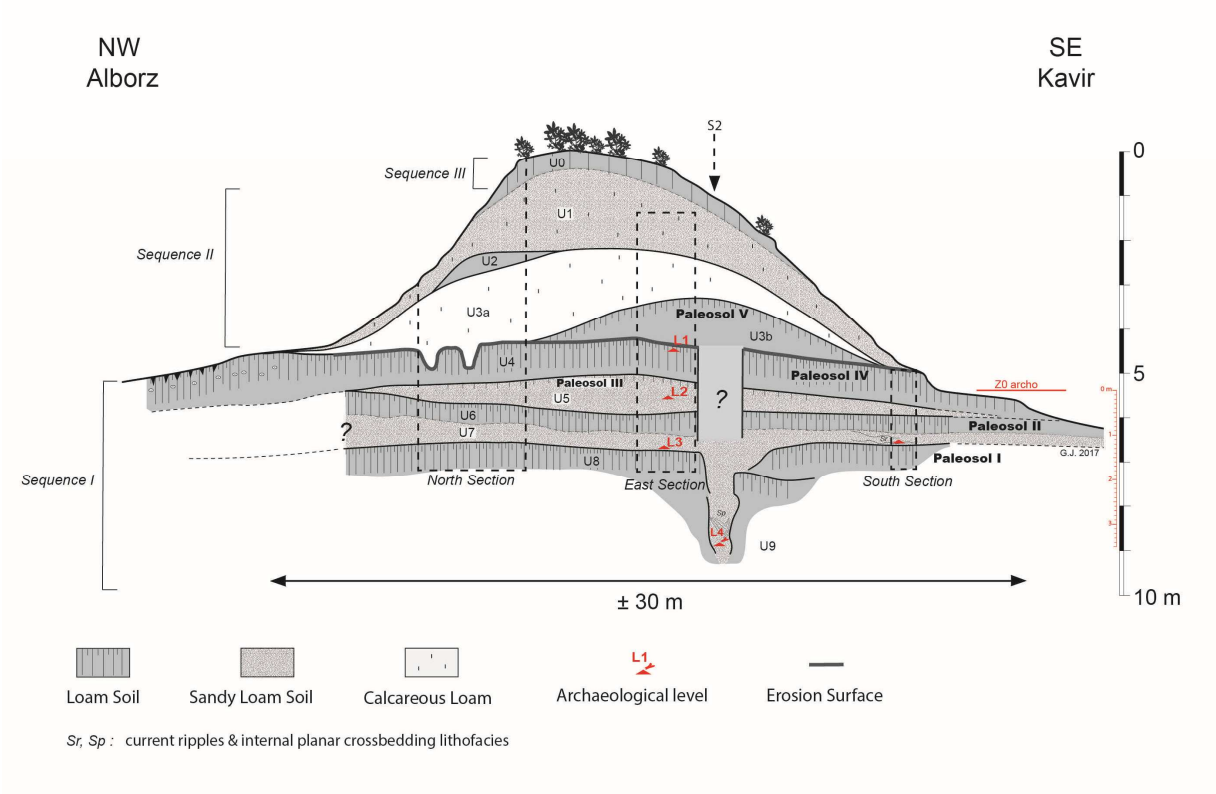

- Figure 9 Pedosedimentary profile of Mirak N°8 (modified from sedim. logs made by Guillaume Jamet, from Berillon et al., 2016).

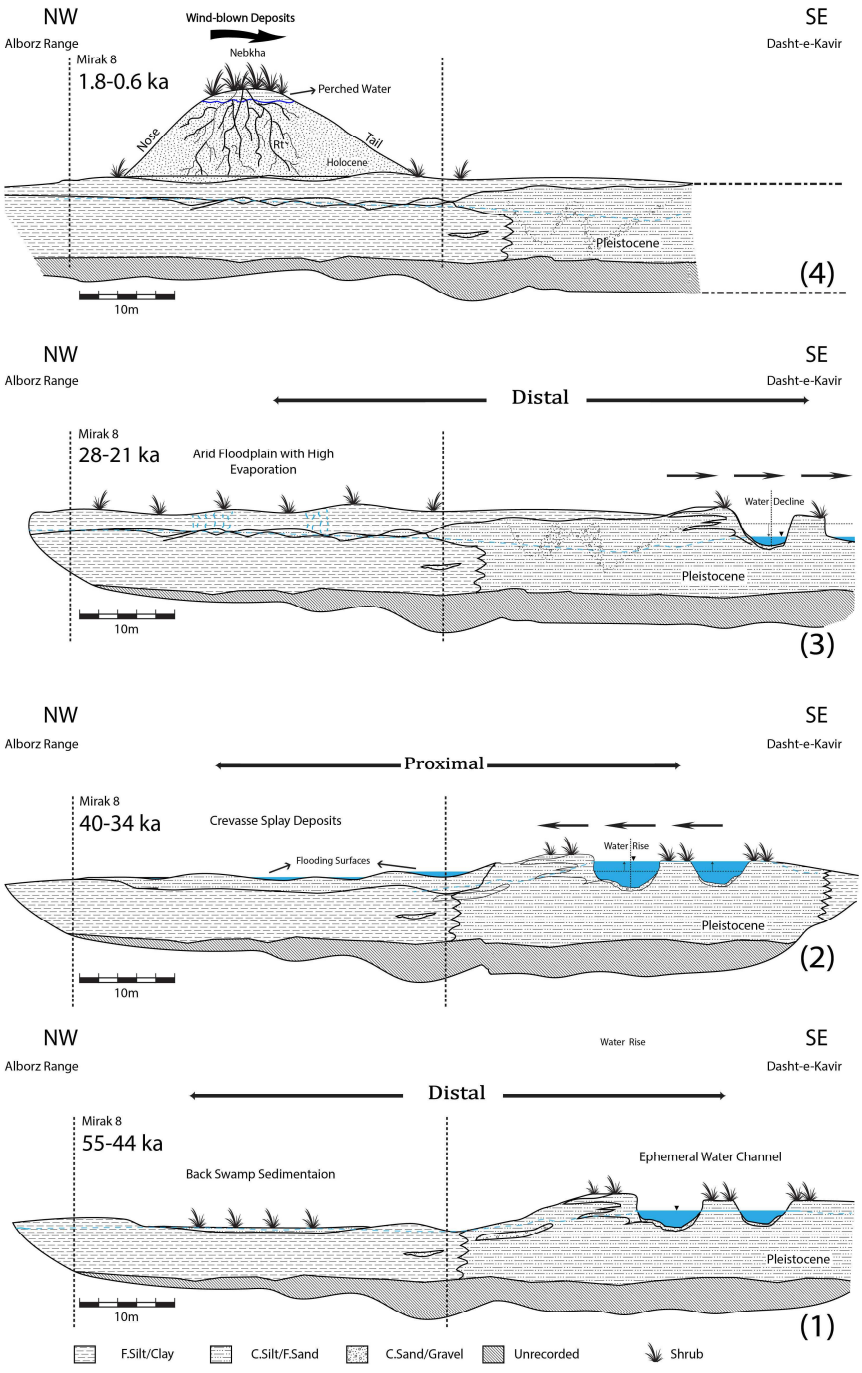

- Figure 10 Simplified diagram of the geological evolution of Mirak N°8; (1): development of old soil successions in unit 8 in a back-swamp environment far from the main fluvial channel. (2): breakage of natural stream levees following the periodic rise in water level and replacement of sand splays in units 7 and 5. (3): protracted period of deflation with no sedimentation after the occurrence of under-developed soil in unit 4 and the eluvial horizon of 4a. (4): burial of Pleistocene palaeosols by advancement of desert loess and dunes during the Holocene.

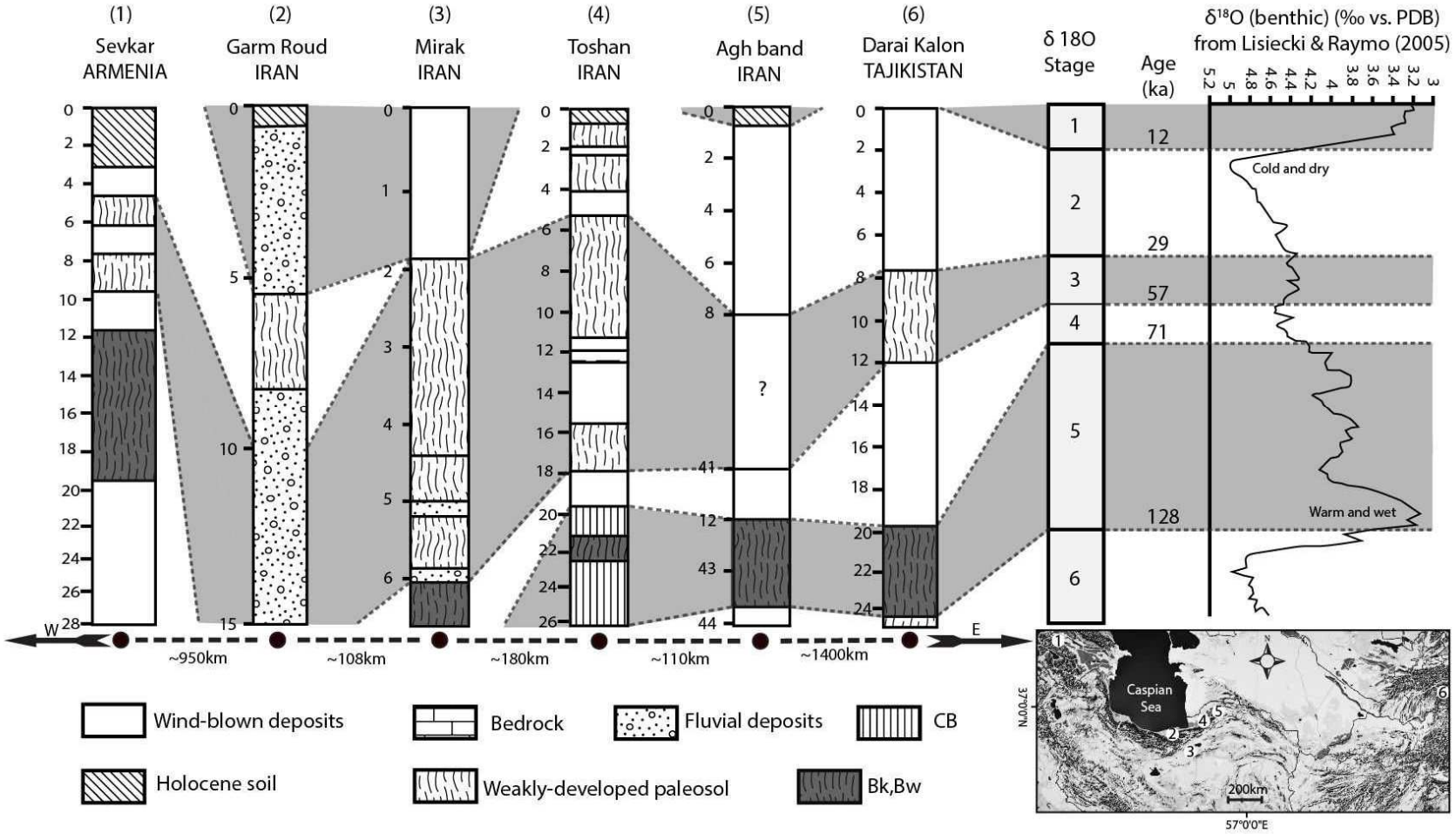

- Figure 11 Chrono-pedostratigraphical correlation of the Mirak record (this study) with a number of other Late Pleistocene/Holocene records.

Table 1 Stratigraphy of the *Mirak N°8* sequence: description of the sampled units and pedo-sedimentary interpretation.

Units	**Macro-scale description**	**Pedosedimentary interpretation**
0	Sandy brown to pink calcareous silt (7.5 YR 7/4) with scaly structure on the surface, lamellar to granular in the middle and massive in the base. Thickness 195 cm.	Modern calcareous silt deposits of wind-blown origin attributable to peri-desert loess.
1	Yellow-brown (10 YR 6/6) calcareous sandy loam. Heterogeneous with no firm pedo-structure and abundant tubular porosities (0.5cm). Contains secondary calcareous nodules. Thickness 5-10 cm.	Under-developed Bk aridisol. Calcareous ground mass, calcareous nodules and coatings are the distinguishing characteristic of these units. These materials are entirely of detritic origin (desert dust) and associated with strong deflation processes in very arid conditions.
2	Very light brown (10 YR 7/4) calcareous sandy loam. Heterogeneous with no firm pedo-structure. Lower boundary is unclear and gradual. Thickness 50 cm.	
3	Very light brown (10 YR 7/4) to red (7.5 YR 7/4) calcareous sandy loam. Unit 3 in the upper part (3a) shows a blocky structure and a homogenous and massive structure in the middle (3b). Abundance of bioturbation in the form of biogalleries and root tracks. Contains black ferro-manganic and carbonate nodules. At the base a small uniform horizon is materialized by a clear green to white (5 Y 8/1) calcareous clay silt, with a massive structure (Unit 3c). Thickness 170 cm.	
4a	Very light brown (10 YR 7/4) to white and light green (5 Y 8/1), compact non calcareous loam with a fine polyhedral structure. Abundance of tubular porosities with long whitish carbonate coatings (calcicutans) and gypsum and salt (Na) coatings inside the fissure porosities. Thickness 40 cm.	Under-developed aridisol. Pedo-features include brown to blackish $$clayey coatings and woody debris in vesicular porosities. In general, all of these features result from an initial vegetated wetland that may have resembled a marsh. The polyhedral to prismatic structure, associated with secondary precipitation (limestone nodules, calcicutans, gypsum, etc.), suggests a polyphased pedogenesis
4b	Light yellow (2.5 Y 7/4) compact non calcareous silt loam. Polyhedral to prismatic structure containing numerous black and oxidized orange ferro-manganic concretions and white calcareous nodules. Thickness 160 cm.	

5	Light yellow (2.5 Y 7/4) to clear grey (2.5 Y 7/2) compact non calcareous sandy loam. Prismatic structure. Containing orange and linear oxidized stains. Thickness 80 cm.	history with desiccation events.
6	Light yellow (2.5 Y 7/4 to clear grey (2.5 Y 7/2) compact and homogenous non calcareous silt loam. Massive structure. Containing numerous bone fragments, root traces and orange and linear oxidized stains. Thickness 80 cm.	Very under-developed aridisol. The massive structure and higher proportion of coarse content in the matrix (fine sand to coarse silt), imply a moderate to strong fluvial dynamic (channel), by which the coarser materials were transported in suspension. Furthermore, intercalations of woody debris imply either erosion of unit 8 or temporary flooding with resumption of plant development.
7	Clear gray (2.5 Y 7/2) compact non-calcareous sandy loam, with massive structure. Abundance of bioturbation in the form of biogalleries (worms/insects) and root tracks. This unit is lenticular and pinches out locally. Thickness less than 40 cm (exact thickness of the unit is hard to determine because of its lens-like characteristic.)	
8	Very light brown (10 YR 7/4) compact non calcareous homogenous loam with prismatic to polyhedral structure. Containing numerous black and oxidized orange ferro-manganic concretions and gypsum coatings. Thickness at least 80 cm	More developed Aridisol strongly affected by post-sedimentary biological activity. Root traces, plant remains and insect bio-galleries, associated with dusty clayey-silty intercalations imply wet post-depositional conditions in a highly vegetated environment (back-swamp). The prismatic structure of the soil and secondary precipitations (e.g. ferro-manganic intercalations and gypsum coatings) in the upper parts are evidence of a secondary $$weathering episode.

Table 2 - Soil micromorphology data for sediments of the Mirak N°8 northern section .

Sample	Unit	Microstructure	Basic mineral components	Secondary mineral components	b-fabric	Voids	Pedo-features	Biominerals	Remarks
Mirak B3/ upper fraction	3	Chn-Chm (Vd)	Qz Si-VdFS SA-SR; Mcr ; Fl SR	Mu; CPx	Stipple speckled-crystallitic	Channels and chamber; few zones with compound packing voids	Co (Mcr) Fw Pass (bioturbation) C Rt and plant remains C Prel Fw N (carbonate) Fw Ex (inside Chn and Rt)	-	Mass fabric is strongly calcareous. Intact and $$weathered detritic carbonate minerals and carbonate impregnations are very dominant. The origin of detritic carbonates may be calcrete, because most of them are micritic and sparites are almost non-existent. Existence of reworked, dissolved and illuviated carbonates indicates wetter conditions.
Mirak B3/ lower fraction	4a	Chn-Chm Vd Cr (weakly separated)	Qz Si-VdFS SA-SR; Fl SR	Mu; CPx	Stipple speckled-crystallitic	Channels and chamber; few zones with compound packing voids	Co (Mcr) Fw Pass (bioturbation) C Rt and plant remains C Ex (inside Chn and Rt)	Bone VFw	Almost all voids seem empty, except for a few voids with micritic or Fe oxide coatings. Emptiness of the voids indicates absence of illuviation from the overlying horizons. Frequent soil nodules of relict soil particles that consist of several grains bound together by calcium carbonate.
Mirak B4/ upper fraction	8 top	Bl Vd	Qz Si SA-SR; Fl SR	Cl; Gy; Mu; CPx	Random-stipple speckled-striated	Plane voids with partially accommodated walls	Co (Gy) Fr N Fw	-	Voids usually coated by gypsum crystals, which may indicate more arid conditions.
Mirak B4/ lower fraction	8	Bl Vd	Qz Si SA-SR; Fl SR	Cl; CPx; Mu; Gy (VFw)	Random-stipple speckled-striated	Plane voids with partially accommodated walls	Co (Gy) Fr N Fw	-	Gypsum coatings are nearly absent and quartz and feldspar are dominant. This may imply wetter conditions that were caused by the presence of condensed bodies of well-sorted and clayey silt deposits beneath these parts that acted as a semi-impenetrable boundary, which could have entrapped and maintained some of the percolating waters in this zone.

Key to table abbreviations (according to Bullock et al., 1985) :

Vd: very dominant; D: dominant; C: common; Fr: frequent; Fw: few; Vfw: very few.
Q: quartz; Fl: feldspar; Cl: calcite; Mu: muscovite, CPx: clinopyroxene; Gy: gypsum; Fr: Iron oxide; Mcr: micrite; Mcs: microsparite.
FS: fine sand; Si: silt; Cl: clay.
A: angular; Ah: anhedral. SA: subangular; SR: subrounded.
Cr: crystallitic; Chn: channel; Chm: chamber, Bl: blocky.
Prel: pedorelicts; Co: coatings; N: nodules; Rt: roots; Pass: passage; Ex: insect excrements.